COMPLEX IMPEDANCE ANALYSIS AND DIELECTRIC PROPERTIES OF BISMUTH SILICON OXIDE (BSO)

by

Prasant Kumar Senapathy

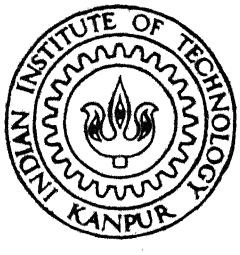

MATERIALS SCIENCE PROGRAMME

INDIAN INSTITUTE OF TECHNOLOGY KANPUR

July, 1997

COMPLEX IMPEDANCE ANALYSIS AND DIELECTRIC PROPERTIES OF BISMUTH SILICON OXIDE (BSO).

A Thesis submitted

in Partial Fulfillment of the Requirement

for the Degree of

Master of Technology

by

Prasant Kumar Senapathy.

to the

MATERIALS SCIENCE PROGRAMME

INDIAN INSTITUTE OF TECHNOLOGY, KANPUR

June 1997

To

“ MAA”

MSP-1997-M-SEN-COM

CERTIFICATE

It is certified that the work contained in this Thesis entitled **"Complex Impedance Analysis and Dielectric Properties of Bismuth Silicon Oxide (BSO)"**, by Prasant Ku. Senapathy, has been carried out under my supervision and that this work has not been submitted elsewhere for a degree.

K. Shahi

K. Shahi

Supervisor

Materials Science Programme

Indian Institute of Technology, Kanpur.

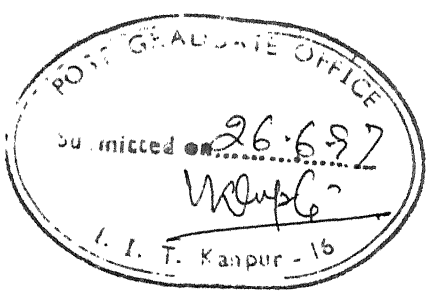

ABSTRACT

Bismuth Silicon Oxide Bi_{12} Si O_{20}, abbreviated as BSO, has attracted considerable attention in recent years because of its potential applications in optical devices, e.g, PROM, etc. However, the basic understanding about its electric and dielectric properties which is crucial for further development is lacking at present. The present project was aimed essentially at contributing towards a better understanding of this important material.

Both polycrystalline specimens and single crystals in pure form as well as doped with Mg and Pr, have been prepared and used for various studies. XRD and SEM studies have been carried out for structural and microstructural characterizations. Our samples confirm to the cubic lattice symmetry with a = 10.15 A^0. The density of single crystal has been measured and found to be fairly close to the reported value 9.20 g/cm^3.

Impedance (Z, θ) measurements on six different samples, viz BSO (pc), BSO:Mg (pc) and BSO:Pr (pc), and three corresponding single crystals, have been carried out over a wide frequency range (5 KHz to 10 MHz) and at different temperatures between 36^0C and 750^0C. The impedance data has been analyzed using the locally developed software package " IONICS" to obtain dc / ac electrical conductivity (σ), dielectric constant (ϵ') and loss factor (ϵ'').

The log σ vs. $10^3/T$ plots for all the samples, pure or doped, polycrystalline or single crystalline, exhibit the characteristics typical of an insulator or semi-insulator; that

is they comprise a low temperature (extrinsic) region wherein the conductivity is practically constant and a high temperature (intrinsic) region in which the σ increases rapidly with increasing temperature. The activation energies in the intrinsic region are in the range 1.1 ~ 1.5 eV. The inclusion of 2 mole % Mg or Pr dopants does not change the conductivity values significantly, but their effect on activation energy is noticeable. This leads us to conclude that Mg and Pr are probably electrically ineffective dopants (like Ge in Si). The above results would suggest a band gap of 2.2 ~ 3.0 eV. for BSO which is in broad agreement with the value obtained from photospectrometry studies (~ 3eV.).

The Dielectric constant ($\in'$) has a fairly high value at low frequencies and decreases uniformly with increasing frequencies. On the other hand, it is practically constant at lower temperatures (at a given frequency), but increases rapidly at higher temperatures. These results suggest the absence of a Debye - type relaxation process in BSO. The effect of impurities / dopants like Mg and Pr on $\in'$ is only nominal.

The dielectric loss ($\in''$) factor has also been investigated as function frequency and temperature. $\in''$ decreases sharply with increasing frequency but the lack of a peak in $\in''$ vs. log f plots confirms the earlier conjecture that there is no Debye - type relaxation mechanism in. BSO.

Acknowledgments

I wish to express my deep sense of gratitude to Dr. K.V Rao, ACMS for introducing me to this new field, providing materials including single crystals and for his overall guidance, and to Prof. K. Shahi for formulation and implementation of the research work, and constant encouragement.

I wish to acknowledge my appreciation to Mr. Dinesh Deva, who was largely responsible for crystals used in this work and for his useful suggestions at different stages in this work. Special thanks goes to my seniors Atanu and Subashish for their cooperation in sorting out many problems in my work and for their brotherly advice which were motivating.

I wish to thank my classmates Guruvinder, Pragya, Manoj, Manoj Kumar for their cooperation and help throughout my M.Tech programme. A word of thanks to my other dept. friends for their ever smiling faces. I also express my sincere thanks to all the staff and members of MSP and ACMS for their help and cooperation.

I sincerely appreciate the companionship of all my Oriya friends who made my stay here really comfortable. My interaction with them academically and otherwise, has always been fruitful and pleasant.

Last but not the least, I thank my family members for their constant source of encouragement throughout this work.

Contents

LIST OF FIGURES

NOTATIONS

BSO: Bismuth Silicon Oxide

sc: Single Crystal

pc: Polycrystal

$Z(\omega)$: Complex Impedance

Z' : Real part of Complex Impedance

Z'' : Imaginary part of Complex Impedance

$Y(\omega)$: Complex Admittance

Y' : Real part of Complex Admittance

Y'' : Imaginary part of Complex Admittance

f: Frequency

R_p: DC Resistance of the sample

σ: DC conductivity

σ_{ac}: AC conductivity

E: Activation energy

E_g: Band gap

σ_0: Pre-exponential factor

ϵ' : Real part of complex permittivity

ϵ'' : Imaginary part of complex permittivity

D: Dissipation Factor

l: Thickness of the sample

A: Area of cross section of the sample

k: Boltz mann constant

Chapter 1

Introduction

The photorefractive effect is now firmly established as one of the highest sensitivity nonlinear optical effects, making it an attractive choice for use in many holographic processing applications. The last ten years have seen an upsurge of interest in photorefractive applications because of several advances in the synthesis and growth of new and sensitive photorefractive materials. Out of all known photorefractive materials bismuth silicon oxide (BSO) is specially important for applications in spatial light modulation, volume holography etc. BSO also exhibits many interesting properties including photoconductive and photorefractive effects. It is these properties together with the dielectric behaviour and resistivity which make BSO an important candidate material for devices like PROM. The literature reports indicate that the limited temperature range of investigation is not sufficient to establish the nature of mobile charge carriers. Thus measurements over a wider temperature range are desirable and only such studies may provide more information to understand the nature of charge carriers, responsible for conduction. Also a literature scan indicates meagre reports on dielectric behaviour of BSO. Moreover, the dielectric behaviour reported by different authors seems to be at variance. The dielectric characteristics are crucial in evaluating the photorefractive performance of BSO for use in the optical devices. In the present project it is desired to

investigate the dielectric behaviour and dc/ac. conductivity of both single crystals and polycrystals over a wide range of frequency and temperature.

1.1 Photorefractive effect:

The photorefractive effect [1-3] can be defined as a light induced change in the optical properties of a material when the incident light has a non-uniform intensity. This non-uniformity is a key feature that distinguishes the photorefractive effect from other common nonlinear effects that occur under uniform intensities. In other words the optical changes are driven by the gradient of the intensity rather than the intensity itself. The main advantage of photorefractive materials is that they require low irradiances in order to generate a significant change in refractive index. As a result power consumption becomes low in optical image processing and optical computing.

The photorefractive effect [4-6] begins with the photogeneration of charge carriers which are free to move. The photogeneration rate is locally a maximum at the positions of maximum intensity. The non-equilibrium photocarrier densities can be driven by diffusion, provided there is no external electric field. When an external electric field is applied the drift dominates the transport.

The second stage of the photorefractive process after photogeneration and tansport is the trapping of charge carriers, forming a space-charge density inside the material. The trapping occurs at the defect sites that are available (empty) to trap charge carriers. When drift dominates the transport under large applied electric fields, the electric field becomes

maximum in the dark fringes as shown in Fig 1.1. On the other hand when diffusion dominates the transport the electric field maxima are shifted by a quarter fringe spacing.

The final stage of photorefractive grating formation process is the conversion of internal space charge electric field into refractive index of the material. This conversion is possible by electro optic-effect. The refractive index of the material can be varied by varying the externally applied electric field. Therefore the spatially modulated light intensity incident on a photorefractive material is converted through the photorefractive process into a spatial modulation of the refractive index with the same spatial frequency as that of the intensity pattern.

Useful photorefractive [7-8] materials should have appropriate material properties. For instance, photorefractive materials must be insulators or semi-insulating semiconductors otherwise excess free carriers screen the trapped space charge. On the other hand the photo refractive materials must have appreciable photoconductivity to allow the charge to separate and to form space charge fields. Defect states with sufficient concentration are essential to the photorefractive process because they provide sites to trap the space charge. When insufficient trap sites are available the space charge fields and the optical gratings are limited in magnitude. Electro-optic effects ultimately determine the magnitude of the light induced gratings. Oxides like $BaTiO_3$, $KNbO_3$,and BSO have large electro-optic effect that makes them attractive for photorefractive applications.

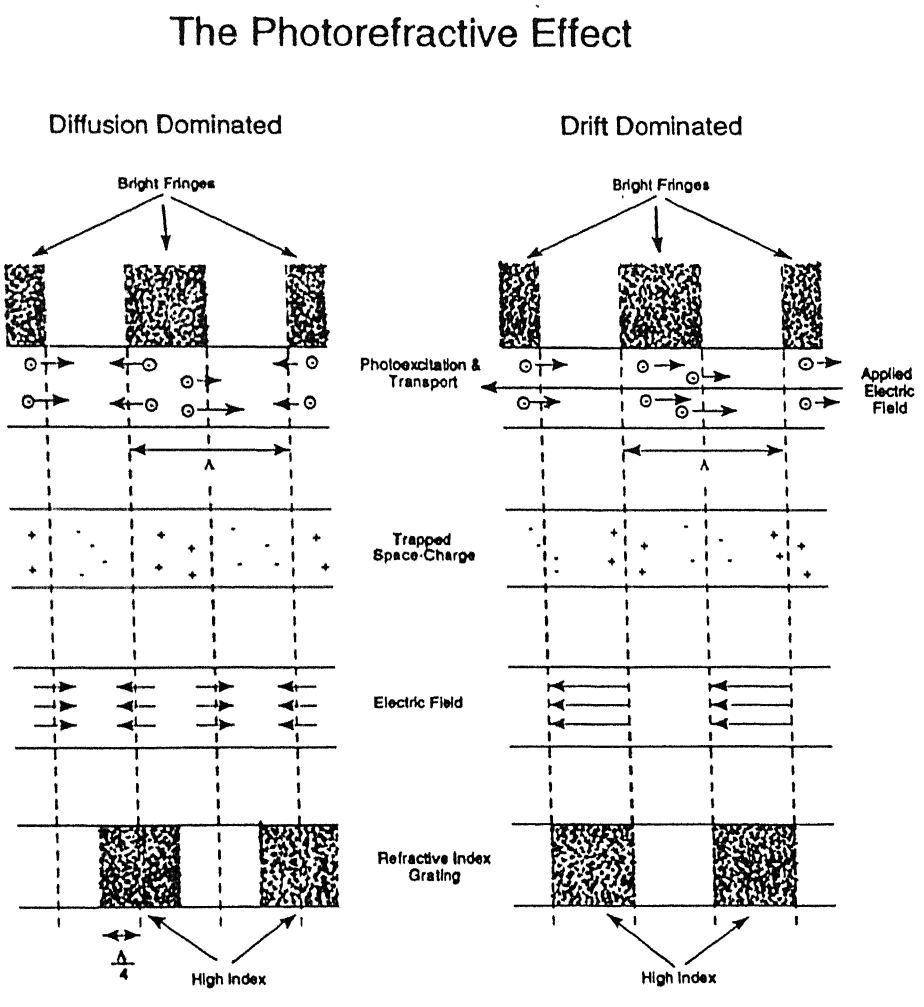

Fig 1.1. The photorefractive process for diffusion dominated and drift dominated transport.

1.2 Behaviour of Defects inside a Crystal:

The photorefractive effect [9-10] depends fundamentally on crystal defects. Once a non-uniform light intensity is incident on a phtorefractive material, photo carriers are ionized out of point defects, which drift or diffuse and are trapped at the defects, forming trapped space charge, i.e, the source of the space charge electric field that mirrors the input light intensity.

Point defects are both cause and culprit for ideal photorefractive behaviour ; control of defects means control of many photorefractive properties. Unfortunately, it has been extremely difficult to control the defects in many of the traditional photorefractive materials. When the translational symmetry of a crystal is broken by a localized flaw in the lattice, the energy levels arise inside the forbidden energy gap of a crystal. The flaw can be a substitutional impurity, an interstitial or a vacancy. Such point defects can also form complexes of multiple point defects. Each of these different types of defects, produce widely different energy levels within the band gap. The vast number of possible point defects and complexes has made it difficult to identify the defect structures that are related to energy levels in the crystals. One of the most important features of photorefractive effect is the operation at very low light intensities. Most nonlinear optical processes require large light intensities, to drive the material into its range of nonlinear response. The variation of internal space charge electric field as a function of photon flux is shown in the Fig.1.2.a. Also the variation of space charge electric field as a function of applied electric field for different acceptor concentrations (N_A), is shown in the Fig.1.2.b.

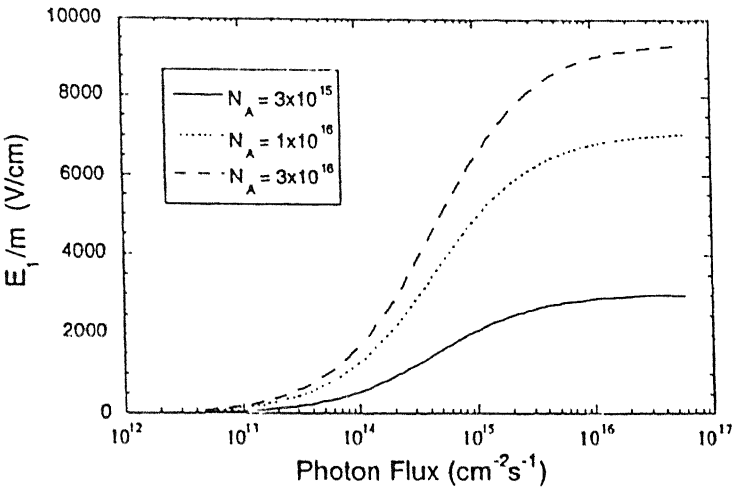

Fig. 1.2.a Variation of space-charge field (E) as a function of photon flux for a constant applied electric field, and different values of acceptor concentrations (N_A).

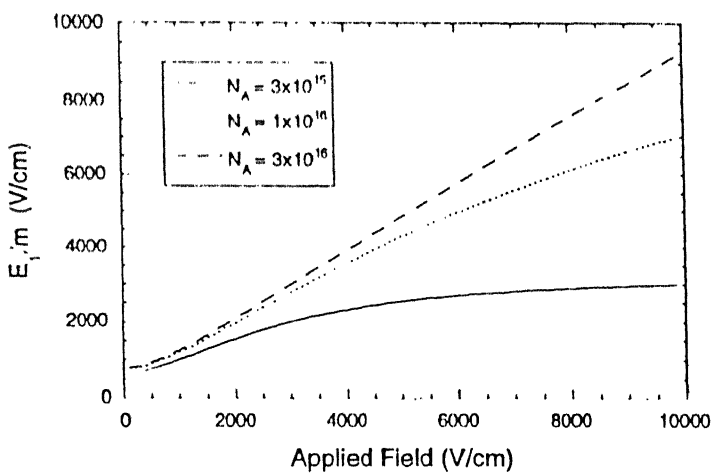

Fig 1.2.b Variation of space-charge electric field (E) as a function of applied electric field for different concentrations of acceptor (N_A).

1.3 Impedance Analysis:

Impedance analysis [11] is a relatively new and powerful method for characterizing many of the electrical properties of the materials. It may be used to investigate the dynamics of bound or mobile charges in the bulk of any kind of solid material (ionic, semiconducting and even insulators/dielectrics). Although much of the experimental work in this Thesis is done at room temperature and above, this analysis can also be applied to the measurement carried out at low temperatures.

1.3.1 Basic Experiment:

For impedance measurement an essential accessory is a cell or a sample holder, which is fitted with a pair of identical electrodes to provide contact with the flat faces of a disc shaped sample. Details of this are given in the next chapter. A multitude of [12-14] fundamental microscopic processes take place throughout the sample when it is electrically stimulated and, in concert, lead to the overall electrical response. They include

(i) the transport of electrons through the electronic conductors.

(ii) the transfer of electrons at the electrode-solid (electrolyte) interfaces to or from charged or uncharged atomic species which originate from the materials and

(iii) the flow of charged atoms via defects in the electrolyte

The flow rate of charged particles depends on the Ohmic resistance of the electrolyte and electrode. The flow of charged particles may be further impeded by the second phase

particles, if any present, at the grain boundaries and by the point defects in bulk of all materials.

1.3.2 Electrical Stimuli Used for Impedance Analysis:

Measuring [15] the impedance by this method is the most common and a standard practice. Here the impedance is measured in frequency domain by applying a single frequency voltage to the interface and measuring the real and imaginary parts of the resulting current at that frequency. Commercial instruments (Impedance Analyzers) are available which measure the impedance as a function of frequency, automatically over a frequency range typically 5Hz to 13.5MHz, and which are easily interfaced to laboratory computers. The advantage of this approach is the availability of these instruments and the ease of their use as well as the experimentalist can control the frequency range to examine the domain of most interest. By the help of this impedance analysis, we can determine the dc/ac electrical conductivity, dielectric constant, energy dissipation factor, etc. of a given material.

1.3.3 Response to a Small Signal Stimulus:

Suppose a time varying signal [16] of frequency ω,

$$V(t) = V_m \sin \omega t \qquad \ldots (1.1)$$

is applied to a sample leading to a current, $I(t) = I_m \sin(\omega t + \theta)$. Where I_m is amplitude and θ is the phase difference between the applied voltage and the current through the sample. Thus the impedance, $Z(\omega)$, of the sample will be,

$$Z(\omega) = \frac{V(t)}{I(t)} \qquad \ldots(1.2)$$

Impedance is a more general concept than resistance because, it takes the phase difference in to account. Expressing the impedance as a complex number,

$$Z(\omega) = Z' + jZ'' \qquad \ldots (1.3)$$

where Z' and Z'' are real and imaginary parts of the Z, respectively i.e,

$$\text{Re}(Z) = Z' = |Z| \cos\theta \qquad \ldots (1.4)$$

$$\text{Im}(Z) = Z'' = |Z| \sin\theta \qquad \ldots (1.5)$$

where phase angle $\theta = \tan^{-1}(Z''/Z')$ and $|Z| = \sqrt{\{(Z')^2 + (Z'')^2\}}$. In general $Z(\omega)$ is frequency dependent as defined above. For complex impedance analysis measurements of Z and θ are done as a function of frequency over a wide frequency range and finally a complex impedance plot, viz, Z' vs. Z'' graph, is used to extract the dc resistance of the sample. There are several other measured and derived quantities, related to impedance which often play important roles in the impedance analysis. All of them may be generically called immitances. One of these immitances is the admittance Y,

$$Y(\omega) = \frac{1}{Z(\omega)} = Y + jY'' \qquad \ldots (1.6)$$

1.3.4 Advantages and limitations:

The impedance [17] analysis has become a popular analytical tool in materials research and development because it involves a relatively simple electrical measurement that can readily be automated and whose results can be correlated with many complex materials variable like conductivity, mass transport, dielectric properties, influence of second phase particles on the conductance of solids, etc. Also it can be used to investigate the membrane of living cells.

The disadvantage of this technique is associated with the possible ambiguities in the interpretation. All electrolytic cells are distributed in space and therefore their microscopic properties may also be independently distributed. Under these conditions, ideal circuit elements may be inadequate to describe the electrical response. Because all the ideal circuit elements represent ideal lumped constant properties. Thus it is often found that the experimental $Z(\omega)$ data cannot be well approximated by the impedance of an equivalent circuit involving only a finite number of ordinary lumped constant elements.

1.3.5 Physical Models for Equivalent Circuit Elements:

If a dielectric material is placed between two metallic plates of a sample holder, then the obtained experimental impedance data, $Z(\omega)$, can be well approximated by the impedance of an equivalent circuit, made up of ideal resistor and capacitor connected in parallel. In such a circuit the resistance represents a conductive path and a given resistor in the circuit accounts the bulk conductivity of the material. Similarly capacitance is generally

associated with the space charge polarization and electro-crystallization process at an electrode. It [15] should be pointed out that ordinary circuit elements such as resistors and capacitors are always considered as lumped constant quantities which involve ideal properties. But in actual practice an ordinary resistor always involves some inductance, capacitance and time-delay response as well as resistance. These residual properties are unimportant over wide frequency ranges and therefore a physical resistor is allowed to be well approximated in an equivalent circuit, by an ideal resistance, one which exhibits only resistance over all frequencies and yields an immediate response to an electrical stimuli.

1.3.6 Dielectric Constant:

A dielectric's [18] qualitative figure of merit is dielectric constant (K). A vacuum provides the reference and by definition has K = 1. The dielectric constant of any other material is expressed as the ratio between the capacitance of a capacitor with that material as dielectric and that using vacuum as dielectric. Mathematically $K = C/C_0$. Dielectric constant is synonymous with relative permittivity ϵ_r. So $K = \epsilon_r = \epsilon/\epsilon_0$, where ϵ_0 is the permittivity of free space (vacuum) and ϵ that of a particular material. The dielectric constant of any material depends on the interaction between an applied electric field and the localized charged centers (molecular dipoles) within the material. Losses in dielectrics primarily result from dielectric absorption, insulation resistance, and the leakage current.

1.3.7 Terms Defining Capacitor Quality:

The various terms [18] which are used to express the capacitor qualities include:

(i) Quality factor(Q)

(ii) Dissipation factor(D)

(.iii.) Power factor

The quality factor Q is [16] 2π times the ratio of maximum energy stored to energy lost per cycle, and is given as,

$$Q = \frac{1}{\omega C_s R_s} \qquad \ldots (1.8)$$

where R_s and C_s are resistor and capacitor respectively in series mode (Fig 1.3a). In terms of parallel mode (Fig 1.3b) the parameter Q is given by,

$$Q = \omega C_p R_p \qquad \ldots (1.9)$$

Dissipation factor is defined as the ratio of the energy dissipated to maximum energy stored per cycle. It is the reciprocal of quality factor Q.

Power factor is defined as the ratio of the energy (or power) lost to input power. In terms of impedance, the power factor is the ratio of capacitor's series resistance R_s to its impedance. It can be shown that,

$$\cos\theta = \frac{R_s}{Z} \qquad . (1.10)$$

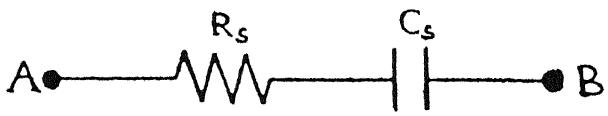

Fig 1.3.a An equivalent series combination of two elements R_s and C_s

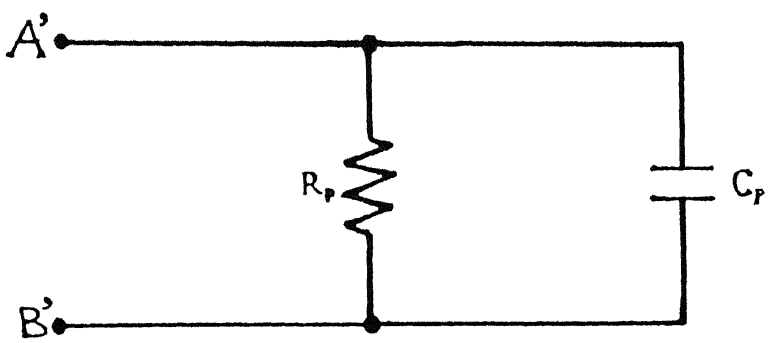

Fig 1.3.b An equivalent parallel combination of two elements R_p and C_p

1.3.8 Equivalent Circuit of a Physical Sample:

When the sample is placed between the electrodes of a sample holder, it can be assumed that the arrangement looks just like a capacitor, having two plates and a dielectric material in between them. The equivalent circuit of such an arrangement (sample between the electrodes) can be expressed as a parallel combination of both resistor R_p and capacitor C_p as shown in the Fig 1.3b. When the experiment is performed for complex impedance analysis, all the measurements are taken under series mode. It means the obtained experimental datas Z and θ, represent impedance and phase angle respectively, for a circuit as shown in the Fig1.3.a. Therefore we can express,

$$Z \cos\theta = R_s \qquad \text{..(1.11)}$$

and

$$Z \sin\theta = \frac{1}{\omega C_s} \qquad \text{..(1.12)}$$

In this way we can get values of R_s and C_s for any particular frequency. However this R_s is not the actual resistance of the sample, and similarly C_s is not the actual capacitance of the sample, at that particular frequency. Thus our aim now is to convert the series circuit, shown in Fig 1.3a into its equivalent parallel combination as shown in Fig 1.3b. It is to be kept in mind that the total impedance across AB and A'B' will be equal, for the two circuits to be equivalent.

Now consider the circuit shown in Fig 1.3 b, where R_p and C_p are connected in parallel. Let the net impedance across A'B' be Z(ω), where frequency dependent Z is given by,

$$Z(\omega) = \frac{R_p}{1 + j\omega C_p R_p} \qquad ..(1.13)$$

The above equation can be written as,

$$Z(\omega) = \frac{R_p}{1 + \omega^2 C_p^2 R_p^2} - \frac{j\omega C_p R_p^2}{1 + \omega^2 C_p^2 R_p^2} \qquad ..(1.14)$$

If Z' and Z'' denote real and imaginary parts of the complex impedance $Z(\omega)$, then we have,

$$Z' = \frac{R_p}{1 + \omega^2 C_p^2 R_p^2} = Z\cos\theta \qquad ..(1.15)$$

$$Z'' = \frac{\omega C_p R_p^2}{1 + \omega^2 C_p^2 R_p^2} = Z\sin\theta \qquad . (1.16)$$

Equations 1.15 and 1.16 yield the ratio,

$$\frac{Z''}{Z'} = \omega C_p R_p \qquad ..(1.17)$$

Now eliminating $\omega C_p R_p$ between the equations 1.15 and 1.17, we get,

$$Z' = \frac{R_p}{1 + \left(\frac{Z''}{Z'}\right)^2} \qquad ..(1.18)$$

or, $$(Z')^2 + (Z'')^2 - R_p Z' = 0 \qquad . (1.19)$$

or, $$\left(Z' - \frac{R_p}{2}\right)^2 + (Z'')^2 = \left(\frac{R_p}{2}\right)^2 \qquad . (1.20)$$

Equation 1.20 represents the equation of a circle on the complex $Z'Z''$ plane, having center at $(\frac{R_p}{2}, 0)$ and a radius of magnitude $\frac{R_p}{2}$.

So if we plot a graph, taking Z' along X axis and Z'' along Y axis, then the plot will be a semi-circle, having a radius of magnitude $\frac{R_p}{2}$. Therefore the diameter of the semicircle gives the value of the resistance R_p. Now the value of C_p can be found out from equation 1.15, corresponding to any point on the semicircular plot as Z', R_p and ω are known. However the value of C_p so obtained is at a particular frequency ω, corresponding to the chosen point on the semicircular plot.

A more accurate value of C_p is obtained from the admittance data (Y and θ) taken at different frequencies. As we know,

$$Y(\omega) = Y' + jY'' \qquad ..(1.21)$$

where $Y' = \frac{1}{R_p} = Y\cos\theta$ and ..(1.22)

$$Y'' = \omega C_p = Y.\sin\theta \qquad ..(1.23)$$

So value of C_p can be found out by dividing Y $\sin\theta$ by ω, where $\omega = 2\pi f$ (f being the frequency). Therefore by measuring the values of Z and θ at different frequencies in series mode and plotting a graph by taking Z' along X axis and Z'' along Y axis, we can get the value of R_p from the diameter of the semicircular plot.

To find out the accurate value of C_p, measurements of Y and θ are taken at different frequencies in parallel mode. The value of C_p at a particular frequency can be found out by dividing Y sinθ by ω.

1.4 Bulk Properties and Electrical Response:

When an electric field is applied [11] to an insulating material, the resulting polarization P may consist of

(.i.) An instantaneous polarization due to the displacement of electrons with respect to nuclei and

(.ii.) A time-dependent polarization due to the orientation of dipoles in the electric field.

If the field remains in place for a long time, the resulting total polarization defines static dielectric constant ϵ_s . On time scales of [15] interest here, i.e longer than 1μs, an applied electric field can interact with a solid in two principal ways. On one hand, the dipoles which are free to rotate will tend to align themselves along the applied electric field. Both energy storage and dissipation are associated with this orientation, leading to the characteristic relaxation times. The dipole moments are normally associated with the complex defects, e.g., an interstitial ion plus a vacancy. On the other hand mobile charges either ionic or electronic will move in response to the field, leading to a conductivity. The charge carriers are usually simple defects such as vacancies, interstitials defects, electrons etc.

The measurement of ionic conductivity, has proved to be the most wide spread application of complex impedance analysis. Because it is possible to eliminate correctly the effects of electrode polarization and at least in some cases the effects of grain boundaries, by proper interpretation of complex impedance.

1.5 Statement of the problem:

In view of the potential application of BSO in optical devices, a through understanding of its basic properties is highly desirable. The following work reported in this Thesis is a small step in that direction.

(.i.) Single crystals and poly-crystalline samples, both pure and doped with Pr and Mg , have been prepared.

(ii) XRD studies and Laue experiment were carried out in order to check the purity of the samples, to determine the lattice parameter and to confirm the symmetry of the lattice.

(.iii.) Complex impedance measurements over a wide frequency range, 5Hz to 12MHz , and at different temperatures, between 36^0C and 750^0C , have been carried out to extract various bulk properties such as electrical conductivity, dielectric constant, loss etc.

(iv) Spectro-photometer experiment has been carried out for measuring the band gap of all the three single crystals.

The organisation of the Thesis is as follows. Chapter 2 has the details of sample preparation and description of experimental setup. Chapter 3 contains results and discussion, and also a brief summary of conclusions drawn and scope for future work.

Chapter 2

Experimental Details

Bismuth Silicon Oxide (BSO), as pointed out in the preceding chapter, has attracted considerable attention in recent years because of its potential applications in modern optical devices. Thus a better understanding of its basic properties, especially electric and dielectric properties, is highly desirable. This Chapter deals with the various experimental techniques used for the synthesis / crystal growth of the material and, electrical and structural characterizations.

2.1 Starting Materials:

The two starting materials required for the synthesis / growth of BSO powder / crystal, are Bi_2O_3 and SiO_2. The used SiO_2 was from Polskie Odizynnike Chenicze Gliwice, Poland (96.5%) and Bi_2O_3 from Aldrich Chemical Co., USA (99.9%). In the final stages the chemicals used were of 5N purity from Morton Thiokol Corp., USA. BSO powder was prepared by fusing together SiO_2 and Bi_2O_3 in the mole ratio 1:6. To prepare doped BSO:Mg and doped BSO:Pr, MgO and Pr_2O_3 were added to the mixture of Bi_2O_3 and SiO_2 by 2 mole %, respectively.

2.2 Preparation of Pellets:

The fine powder of each composition (pure BSO or BSO doped with Mg or Pr) was transferred to a stainless steel die as shown in Fig 2.1. After leveling the powder by die-piston, the whole assembly was placed in a hand-operated hydraulic press. Pressure used in all cases was ~ 4 tons/cm^2. The piston diameter fixed the diameter of pellets at ~ 1.1 cm, while the thickness of the pellets usually ranged between 1.1 to 1.3 mm. The compacted mixture or pellet was then heated at a temperature of ~ 450^{0}C for about 8 hrs. Thorough cleaning of the die with acetone was observed as a usual practice. Pellets then obtained were kept in small specimen bottles which in turn were stored in vacuum desiccator, for further use.

2.3 Growth of Single Crystals:

Bismuth Silicon Oxide crystals can be grown by hydro-thermal and melt methods. The most popular method is the Czochralski technique and the furnaces employed are either resistance heated or radio frequency heated ones. The furnace used in our lab, for growing the crystal is a resistance heated one. Suitable rates of pull and rotation had to be maintained to grow crystals of good quality. Due to the corrosive nature of the material, and in order to maintain the requisite purity of the crystals, platinum crucible was used for holding the melt.

2.3.1 Seed Preparation:

The first step in the growth of single crystals is the growth and preparation of seed

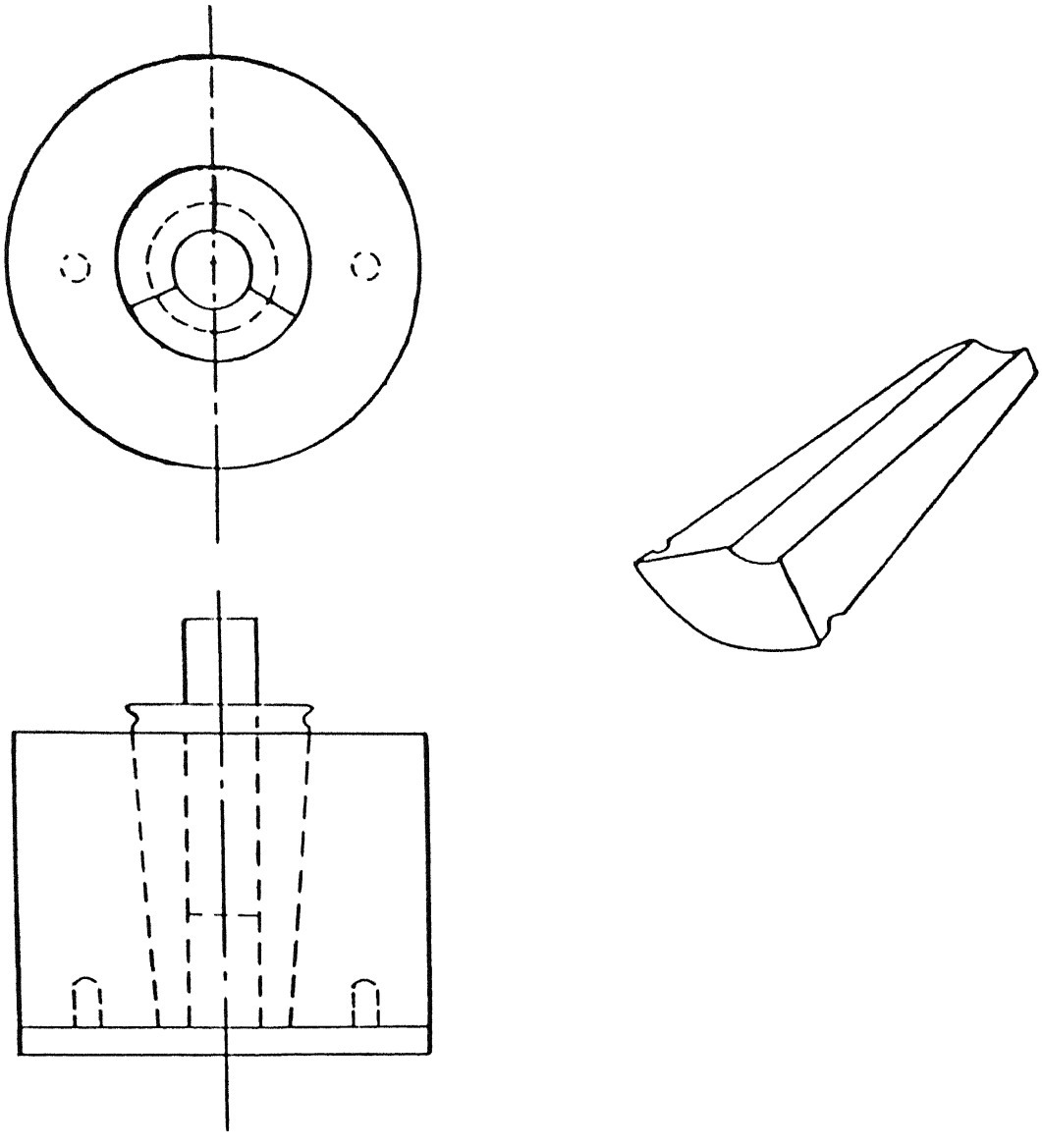

Fig 2.1 Stainless steel die used for making pellets.

crystals. This is a very labourious process. The initial preparation of the seed is attempted by dipping a platinum wire and pulling it out from the melt. Each time a visually acceptable crystal was obtained and it was tested by X-Ray diffraction. Suitable portions were then cut out and subsequently used as seed material. This chain process was repeated a number of times till a good seed crystal was obtained. The first few trials were made with platinum wire of about 0.3mm diameter. It was deliberately attempted, by adjusting the rate of pull and temperature to make the resulting solid piece as conical as possible or in other words to get a single crystalline grain at the bottom which is then used as a seed.

2.3.2 Pulling and Rotation Systems:

For good quality crystal a pulling rate of ~ 2.5-6 mm/hr and a rotation rate of 25 ~ 45 rpm is used. Many techniques have been used to control the stepper motors, regarding the above matter. For growing the crystal in our laboratory, the rotation rate and pulling rate were kept at 30 rpm and 4 mm/hr respectively.

2.3.3 Furnace:

The resistance wire wound furnaces, described in the literature for the growth of BSO crystal, utilise a three-zone heating system consisting of (from bottom upwards) a guard zone, a melt zone and an annealing zone. This arrangement is desirable since BSO has a high thermal expansion and low thermal conductivity. Thus the thermal gradients can produce internal stresses which in turn can lead to the formation of cracks etc. A

three-zone furnace has been designed and fabricated in our laboratory to be used with pulling and rotation system.

2.3.4 Crystal Growth:

Pure BSO boules were pulled from the melt in our laboratory in a specially fabricated Czochralski growth system in air. The crystals were grown using platinum crucible and kanthal wire wound furnace. A stoichiometric mixture of Bi_2O_3 and SiO_2 powders in the ratio 6:1 were used for growing pure BSO crystals. During the growth process the pulling and rotation rates were kept at ~ 4 mm/hr, and ~ 30 rpm respectively. The crystal boule was oriented by the X-Ray method and from it slices of about 1mm thick and area of 100 mm^2 was cut along a particular plane. The two flat faces of the sample (crystal) were coated with silver paint and then it was introduced into the sample holder for taking measurements.

It should be noted that a failure in the crystal growth can result not only in the wastage of the material and time but also the loss of seed crystal itself. Therefore it is necessary to have at least three prepared seed crystals readily at hand all the times. In spite of these precautions, power supply problem did sometimes cause the loss of all seed crystals; making it necessary to go back to the earlier stage. However this problem can be overcome by using UPS system.

2.3.5 Crystal Cutting, Grinding, and Polishing:

The single crystals grown above were cut with a Metals Research Microslice-2

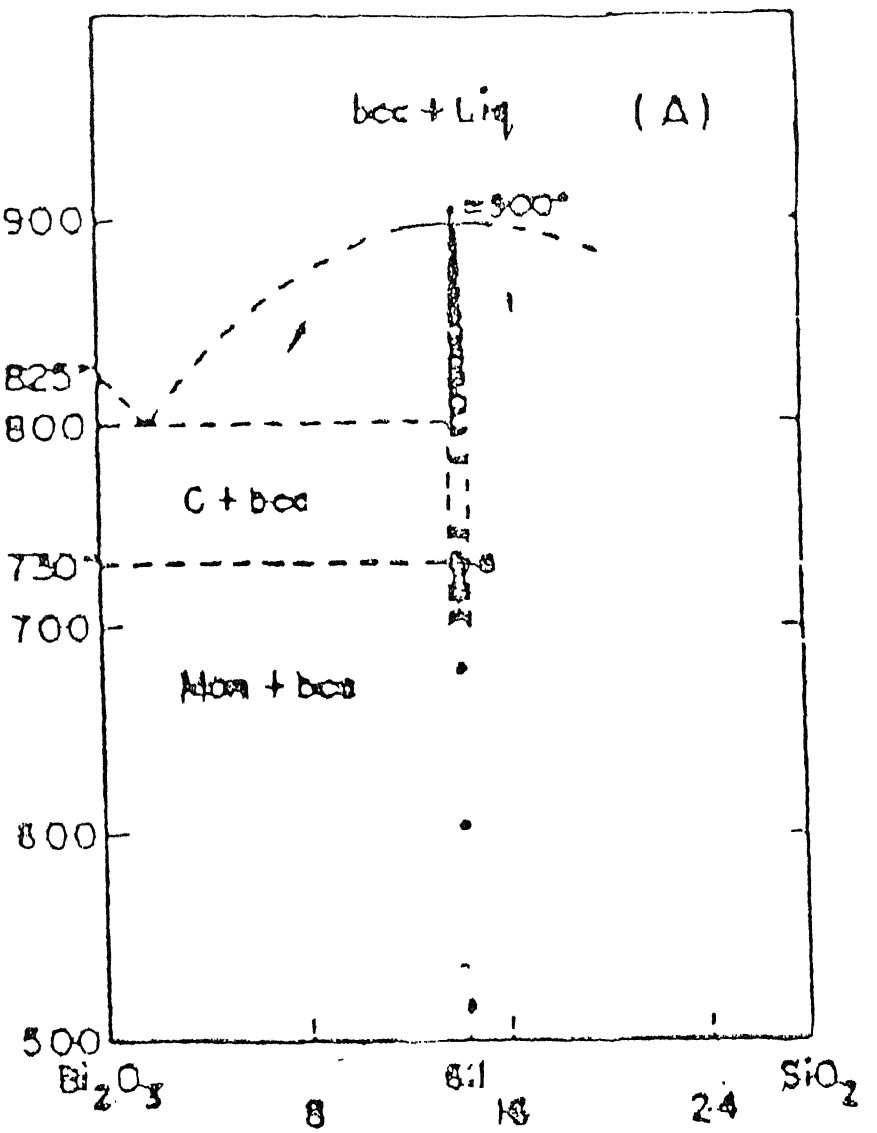

Fig. 2.1.a Complete phase diagram of Bi_2O_3 - SiO_2 system.

crystal cutter, employing a very thin (50 μm) diamond impregnated blade. The crystals are usually mounted in wax. After cutting the crystal, it is removed carefully, by warming the base. Due to the brittle nature of the material and thermal stress problems, great care has to be exercised during this process. The cut crystal is then ground on a glass plate with various grades of silicon carbide powder and the final polishing was done on a rotating aluminium base fitted with polishing cloth, loaded with γ - alumina.

2.4 Impedance Measurement:

The electrical conductivity measurements as a function of temperature requires a furnace, a sample holder, a temperature controller and an impedance bridge. These are briefly mentioned below.

2.4.1 Furnace:

Kanthal wire of 1.5 mm diameter was wound inductively and uniformly at the rate of 10 turns per inch, on a mullite tube (18 inches in length and 2.25 inches in diameter). The total resistance of the heating element is ~ 34 Ohms. A layer of pellendum fire cement is so applied over the heating element that no kanthal wire is visible from outside. The cement is first allowed to dry at room temperature and then at 100^0C-150^0C inside the oven. The mullite tube wound with kanthal wire is housed in a cylindrical aluminium construction, which is open at both ends. Two asbestos plates were used to cover the two flat ends of the furnace and were fixed in place with screws. The space between the mullite tube and the aluminium enclosure was filled with asbestos powder to reduce the heat loss.

2.4.2 Sample Holder:

The Fig 2.2 shows the general sample holder used for two probe resistivity and capacitance measurements above room temperature. The lava discs which can be moved smoothly along the two parallel stainless steel support rods, in combination with the spring and the quartz tube, applies uniform pressure to ensure a firm contact between the electrodes and the sample. The length of the sample holder is such that the spring is located outside the furnace, so that it can maintain its spring constant. Platinum foils were used as electrodes. Platinum wires welded at the back of each electrodes, served as electrical lead wire. A cromel versus alumel (Type K) thermocouple was used to monitor the temperature.

2.4.3 The Experimental Set-up:

This work involved extensive electrical conductivity measurements. A block diagram of the set-up used is given in Fig 2.3. Temperature inside the furnace was controlled by a combination of temperature controller and a thermal relay. A Keithley microvolt DMM (model HIL-2301) was used to measure the thermocouple voltage and hence the temperature. HP 4192A Low Frequency Impedance Analyzer was used for impedance measurements at various temperatures. This instrument has a wide range of frequency; 5Hz to 13MHz. The surface of the sample was silver painted, in order to avoid the air gap effect between the electrode and the sample, when the latter is loaded in the sample holder. The tip of the chromel-alumel thermocouple was placed as close to the sample as possible to measure as well as to control the temperature of the sample. For

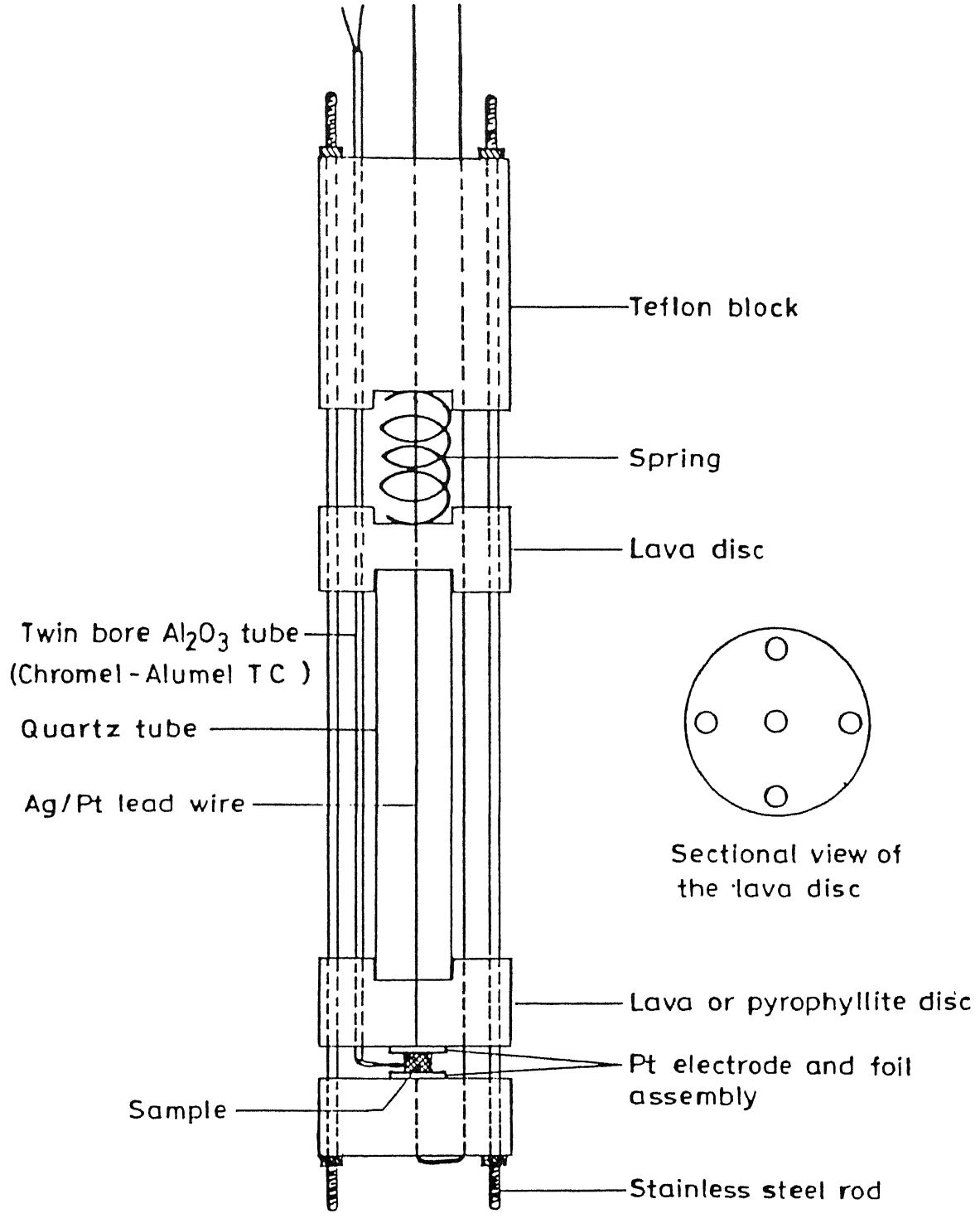

Fig 2.2 Sample holder for two-probe resistivity and capacitance measurements in the temperature range 300K~1000K.

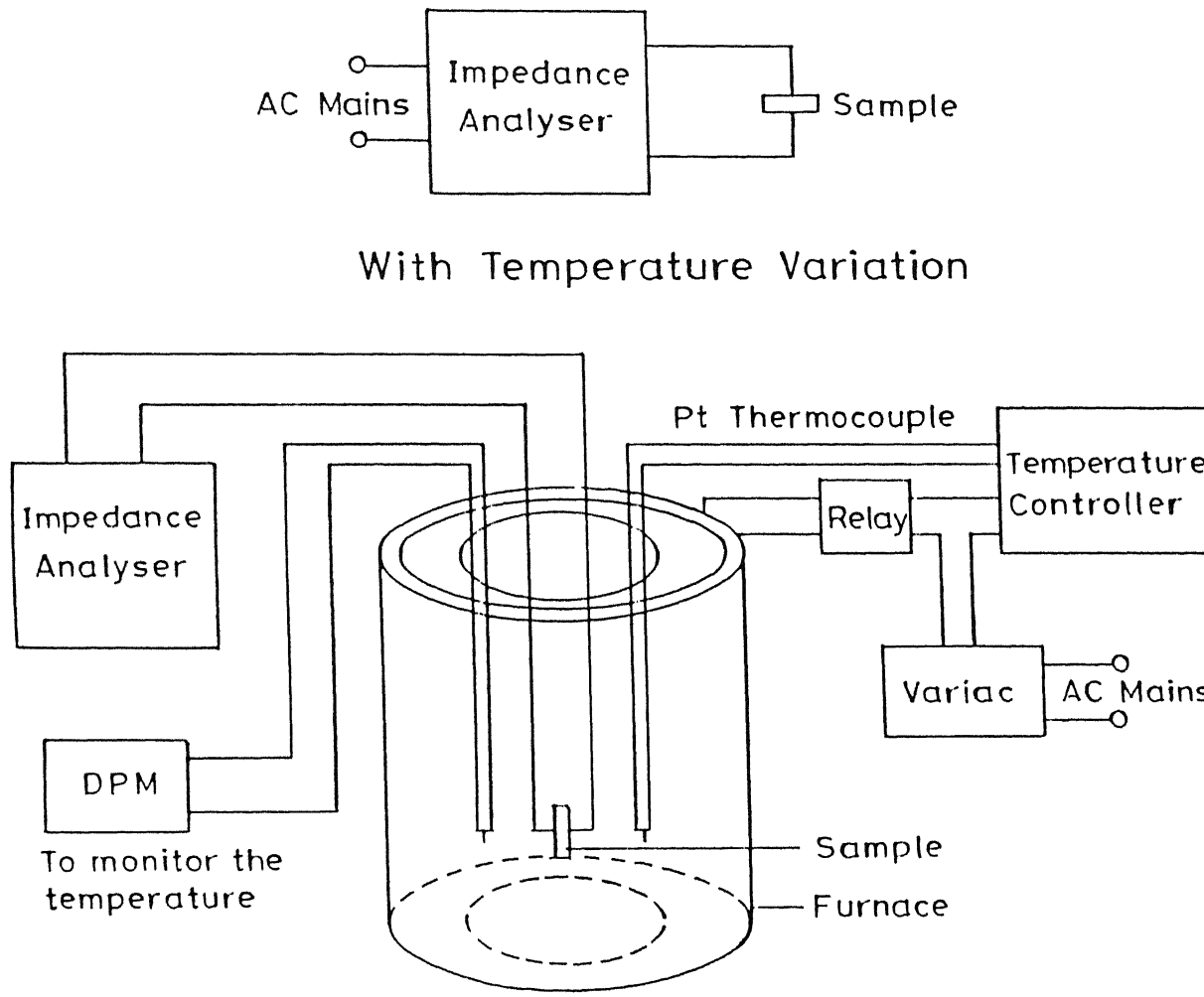

Fig 2.3 Schematic diagram of the set-up used for impedance measurements.

each sample the temperature was increased from room temperature to 750^0C and at each temperature, values of Z, θ or Y, θ were measured at different frequencies.

2.4.4 Complex Impedance Analysis:

The HP-4192A Low Frequency Impedance Analyzer can accurately measure the impedance parameters of a component or a circuit at various frequencies, test signal levels and dc bias levels. The ranges available are:

(.i.) measuring frequency: 5Hz to 13MHz .

(.ii.) OSC level: 5mV to 1.1V (rms.).

(.iii.) DC bias voltage: -35 to +35V.

Frequency of the signal and bias voltage can be manually swept, full range, in either direction. OSC level can also be swept (manual only) at 1mV steps.

For connecting the sample to be tested, the HP-4192A employs measurement terminals in a four terminal pair configuration which has a significant measuring advantage for component parameter requiring high accuracy in the high frequency region. Generally any mutual inductance, interference of the measurement signals, and unwanted residual factors in the connection method which are incidental to ordinary terminal methods significantly affect the measurement at higher frequencies. The four terminal pair configuration measurement permits easy, stable and accurate measurements and avoids the measurement limitations inherent in such effects. The four terminal pair configuration consists of four connectors: High current (H_{cur}), High potential (H_{pot}), Low current (L_{cur}). and Low potential(L_{pot}). The purpose current terminal is to cause a measurement signal current to flow through the device under test or sample. The potential

terminals are for detecting the voltage drop across the sample. The main principle is that, the signal current does not develop an inductive magnetic field and thus the test leads do not contribute additional measurement errors due to self or mutual inductance between the individual leads. However the four terminal system must be converted to a two terminal configuration, because the sample under test has two leads.

The impedance of a component can be expressed in vector representation by a complex number as shown in Fig 2.4. In such a representation, the effective resistance and the effective reactance correspond to the projections of the impedance vector ($Z\angle\theta$) on the real axis (R) and imaginary axis (jX) respectively. The measurements taken by this instrument were then analyzed by using complex impedance plots.

2.4.5 Complex Impedance Plot:

Complex impedance plots are useful for determining an appropriate equivalent circuit for a system and for estimating the values of circuit parameters. The complex impedance $Z(\omega)$ of a system at an applied angular frequency ω, can be expressed as,

$$Z(\omega) = Z' + jZ'' \qquad \text{....(2.1)}$$

The impedance was measured by Impedance Analyzer over frequency ranges 5kHz to 10MHz. The impedance data thus obtained was then analyzed by using the package IONICS, developed locally by S.Bhatnagar, [19] in the "Solid State Ionics" laboratory. This package plots the imaginary part of the impedance versus real part and the obtained resulting locus shows distinctive features for certain combinations of circuit elements.

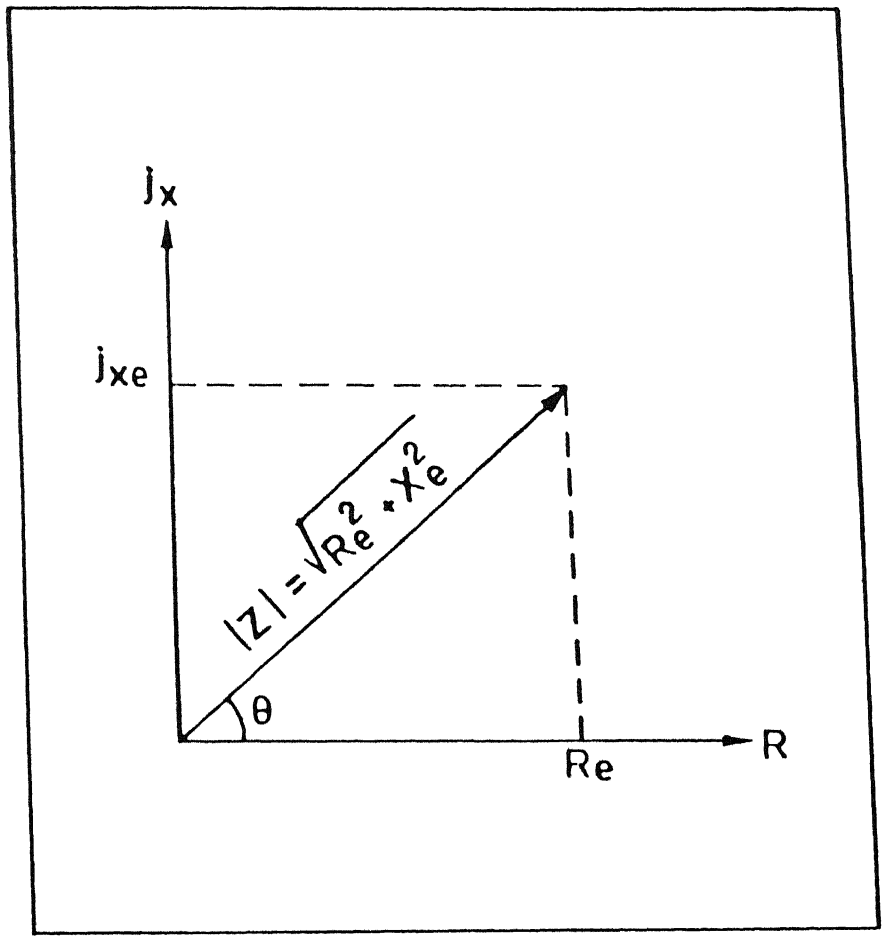

Fig 2.4 Vector representation of an Impedance.

2.5 Density Measurements:

Density of the pellets was determined using the formula and procedure given below,

$$\text{Density} = \rho_w \left(\frac{W_1}{W_2 - W_3} \right) \qquad \text{....(2.2)}$$

where

ρ_w = density of water

W_1 = weight of the pellet in air

W_2 = weight of the pellet taking out from the distilled water + weight of the wire.

W_3 = weight of the pellet in water + weight of the suspension wire.

At first the weight (W_1) of the sample whose density is to be determined, was measured with help of an electric balance. Then the sample was tied with a wire and inserted into a beaker filled with distilled water. The beaker was then placed in a vacuum desiccator for ~ 1.5 hrs. The weight W_3 was now measured following the same procedure as before. The pellet was then taken out from the beaker, and its weight W_2 was again measured along with the wire with the help of electric balance. Density of distilled water was taken as 1.0 gm/cm^3 and by using the above equation the density of the pellets were determined.

2.6 Spectrophotometer Experiment:

This experiment was performed, in order to determine the band-gap of the BSO

single crystals. The instrument used for this is a Double Beam Spectrophotometer Hitachi, model 150-20. The above experiment can also be used for the measurement of absorption and transmittance of liquid, solid and gaseous samples in Ultra Violet, Visible and near Infra-red regions. In our case the experiment was performed in Ultra-Violet and Visible regions.

2.7 X-Ray Diffraction (XRD):

X-Ray diffraction patterns of the samples have been recorded using a Rich Seifert (ISO-Debyeflex 200 2D) counter diffractometer employing a filtered C_uK_α radiation (λ = 1.542 A^0).The generator was operated at 30KV and 20mA. The chart speed was fixed at 30 mm/minute and the scanning speed was 0.3 degree/minute in 2θ. All XRD studies were done at room temperature (36^0C). For powders, the sample films were fixed on glass slides with a drop of methanol.

2.8 Laue's Experiment:

The Laue method was the first diffraction method ever used, and it produces Von Laue's original experiment. A beam white radiation, the continuos spectrum from an X-Ray tube, is allowed to fall on a single crystal. The Bragg angle θ is therefore fixed for every set of planes in the Crystal, and each set picks out and diffracts that particular wavelength which satisfies the Bragg law for the particular values of 'd' and 'θ' involved. Each diffracted beam thus has a different wave-length.

In the present work, the back-reflection Laue method was performed. The film was placed between the crystal and the X-Ray source. The incident beam passing through a hole in the film, was allowed to fall on the crystal. The beams diffracted in the back-ward direction were recorded.

2.9 Scanning Electron Microscopy (SEM) :

The scanning electron microscopy (SEM) is the most powerful tool to study the surface topography and morphology with an unprecedented advantage of depth of field and a capability of studying any surface in its original unaltered state. From the standpoint of actual microscopy, the scanning electron microscopy images topographical details with maximum contrast and depth of field by the detection, amplification and display of secondary electrons.

The samples for SEM measurement were prepared by breaking small portions from the pellets. The pieces were then mounted on a brass stub with Duco cement and painting silver paint around the edge of the specimen and the stub. Then they were transferred to a vacuum jar and coated with conducting layer of silver by vacuum deposition. Then the specimens were ready for SEM observations.

Chapter 3

Results and Discussion

The work presented in this chapter is a part of the systematic ongoing studies on dielectric materials in our laboratory. As pointed out earlier, Bismuth Silicon Oxide, $Bi_{12}SiO_{20}$ (abbreviated as BSO) has attracted considerable attention in recent years because of its potential applications in various optical devices such as PROM etc. Table 3.1 summaries the general properties of BSO.

Table 3.1

General Properties of BSO [20]

Chemical Composition	Bi_{12} Si O_{20}
Symmetry	Body Centered Cubic
Point Group	23
Index of Refraction (for $\lambda = 0.633$ μm)	2.54
Transparency (%)	70
Density (gm/cm^3)	9.2
Lattice Parameter (A^0)	10.103
Electro Optic Coefficient (γ_{41})	5×10^{-10} cm / V
Optical Activity (for $\lambda = 0.633$ μm)	22^0 / mm

In spite of several studies on BSO, it appears that its electric and dielectric properties are not well understood at present. With a view to contribute towards a better understanding of this material, we have carried out the investigation on the pressed pellets and single crystals grown locally, as well as on samples doped with Mg. and Pr. In particular the following measurements have been carried out and presented in that order.

(i) Structural characterization of the pure and Mg / Pr doped powder samples and single crystals at room temperature.

(ii) Microstructure by SEM

(iii) Density Measurements

(iv) Impedance analysis leading to (a) dc electrical conductivity σ (b) ac electrical conductivity σ_{ac} (c) dielectric constant (ϵ') and loss (ϵ'') vs temperature (300^0C ~ 750^0C) and frequency (5KHz ~ 10 MHz).

(v) Spectrophotometric experiment.

3.1 Structural Characterization:

A total of six samples, viz, BSO (pc), BSO:Mg (pc) and BSO:Pr (pc), and BSO (sc), BSO:Mg (sc) and BSO:Pr (sc), have been investigated by us in this Thesis. X-Ray diffraction (XRD) measurements (for experimental details, see Section 2.7) were carried out at room temperature on two of the above samples, viz, pure BSO in form of powder and pressed pellet, and BSO single crystal. The results are shown in Figs 3.1 (a), (b) and 3.2.

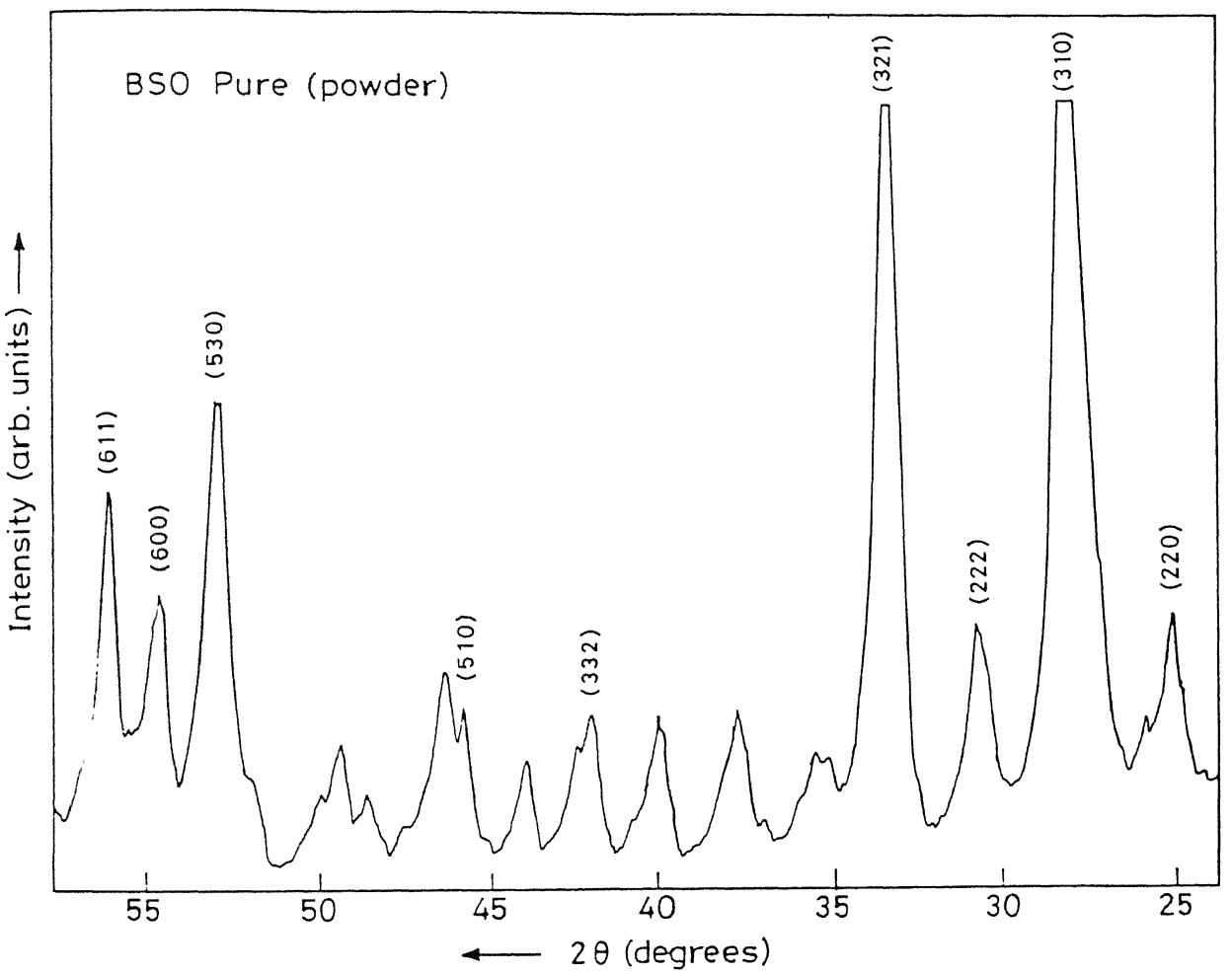

Fig 3.1.a XRD pattern for pure BSO powder.

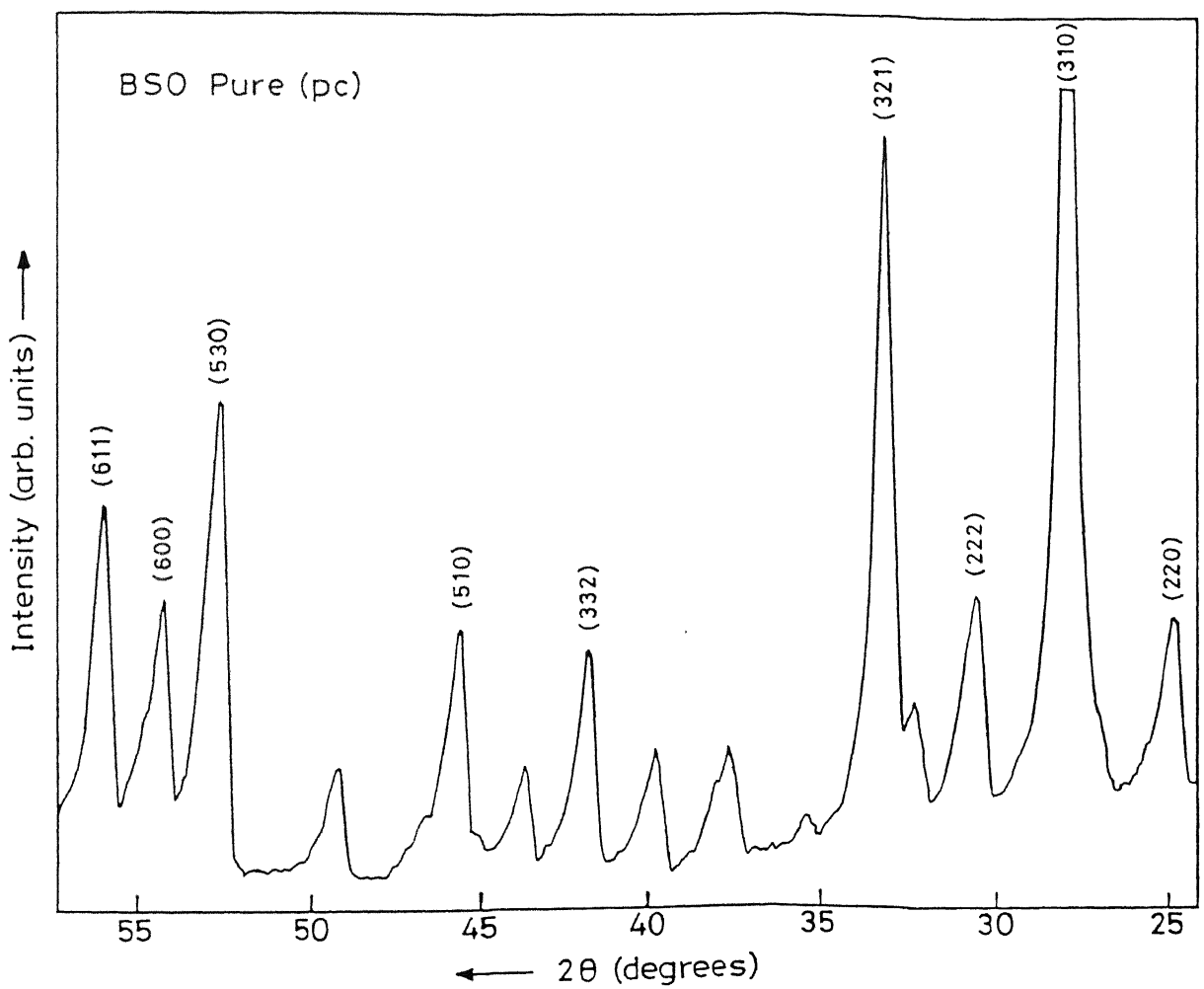

Fig 3.1.b XRD pattern for pure BSO polycrystal (pc).

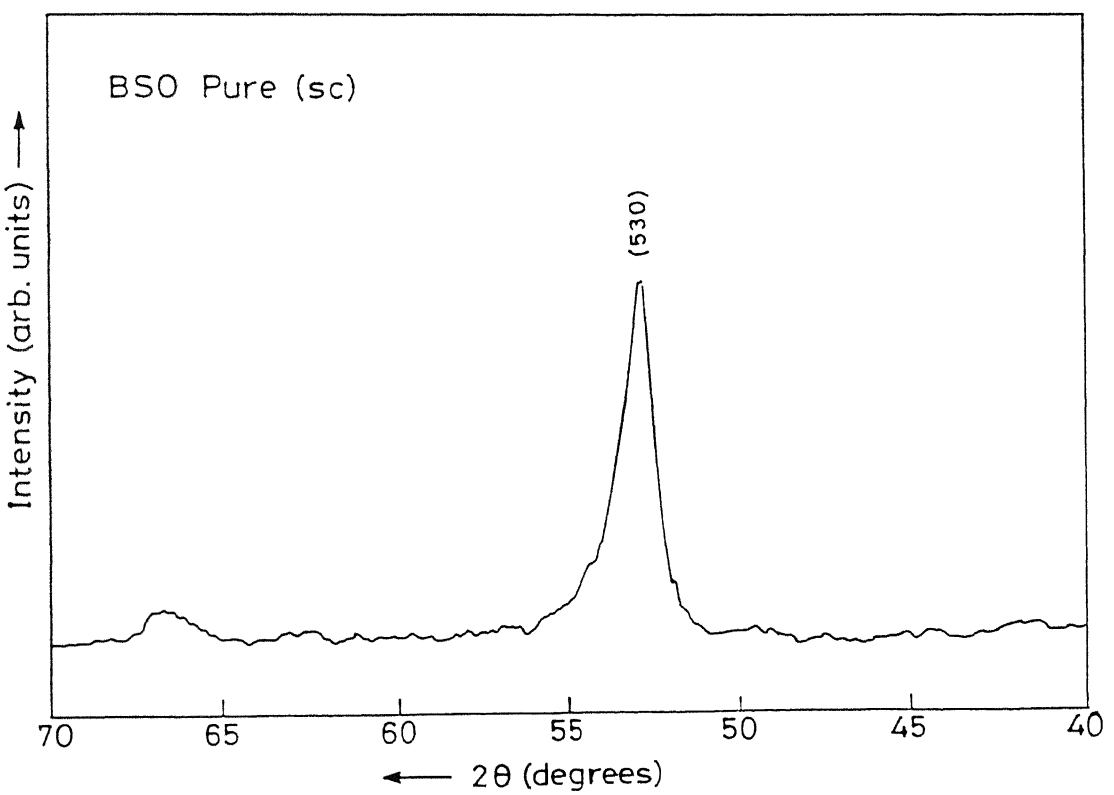

Fig 3.2 XRD pattern for pure BSO single crystal (sc).

The XRD patterns for the BSO powder and pressed pellet (Figs 3.1.a and 3.1.b) are in very good agreement with each other as expected. The only noticeable difference is that the intensities of some of the peaks for powder sample are somewhat larger than those for the pellet sample (Fig 3.1.b). The various peaks observed in Figs 3.1.a and 3.1.b for powder samples have been indexed. Both relative intensities as well as 2θ values observed for our samples are in reasonable agreement with those reported in literature [21-23] (Table 3.2).

Table 3.2

Powder Diffraction Data on BSO [22-23]

2θ	Intensity	h k l
24.921	30	2 2 0
27.858	100	3 1 0
30.591	30	2 2 2
33.027	90	3 2 1
37.768	20	4 1 1
39.856	15	4 2 0
41.989	20	3 3 2
49.383	14	5 2 1
52.781	55	5 3 0
54.442	25	6 0 0
56.216	35	6 1 1

From the obtained XRD pattern, the lattice constant is found to be 10.15 A^0, while the literature [23] value is 10.103 A^0. Fig 3.2 shows XRD pattern for pure BSO single crystal which exhibits a single peak at $2\theta \sim 52.8^0$ corresponding to the crystal plane (530). Reflections may take place from other crystallographic planes [24], but no peaks may result because of the cancellation of scattered X-rays as these are out of phase.

There is some controversy regarding the composition of BSO, as to whether it is Bi_{12} Si O_{20} or Bi_{24} Si_2 O_{40}, i.e, (Bi_{12} Si O_{20})$_2$. It is observed that, the crystals grown confirm to Bi_{24} Si_2 O_{40} and this is normally referred to as BSO, and the molecular formula is given as Bi_{12} Si O_{20}.

Laue's back-reflection experiment was performed on pure BSO single crystal. The results are contained in the photograph shown in Fig 3.3. The spots are seen to lie on certain curves. These curves are generally hyperbolas. Spots lying on any one curve [24] are reflections from planes belonging to one zone. This is due to the fact that the Laue reflections from planes of a zone all lie on the surface of an imaginary cone, whose axis is the zone axis. The bright spots [25] are due to the superposition of different orders of reflection from a particular plane.

3.2 Microstructural Studies:

The SEM micrographs are displayed in Fig 3.4.a and 3.4.b. From Fig 3.4.a it is clear that there is a considerable grain growth in case of pure BSO pellet, while the grain size is found to be smaller for a BSO:Mg pellet. From this it can be concluded that the dopant present inside the BSO:Mg pellet may cause hindrance to grain growth.

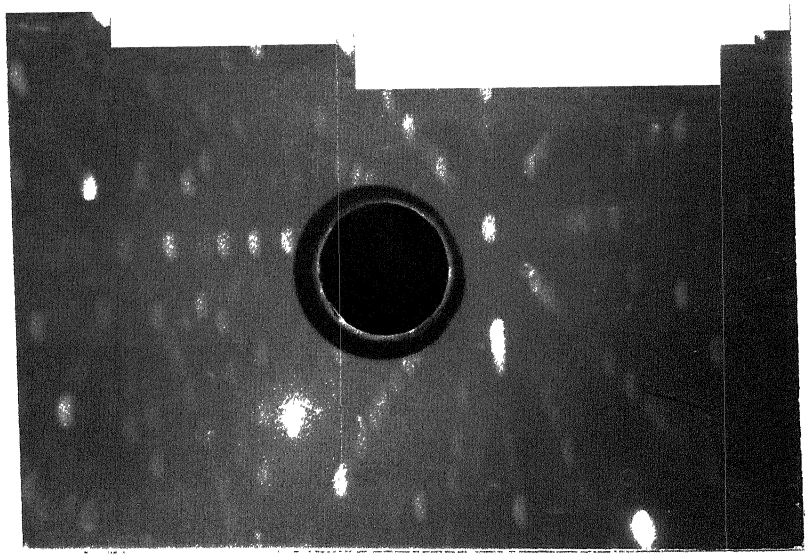

Fig 3.3 Laue pattern of a BSO pure (sc) in approximately the [100] orientation.

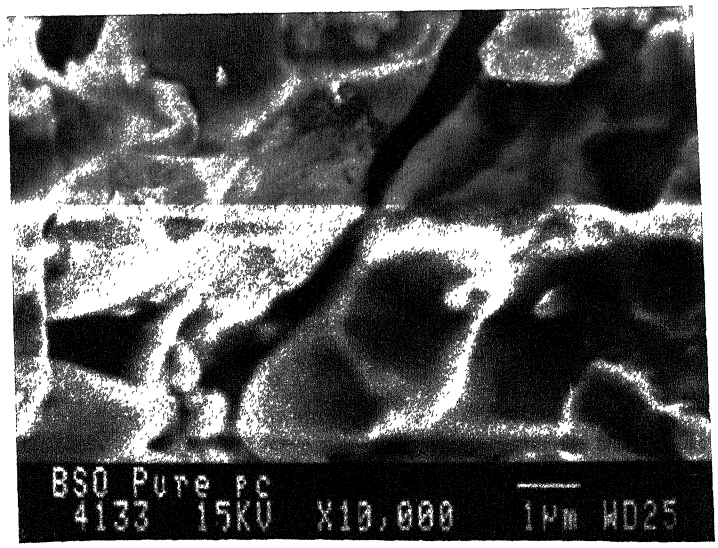

Fig 3.4.a SEM micrograph for a pure BSO pressed pellet (pc).

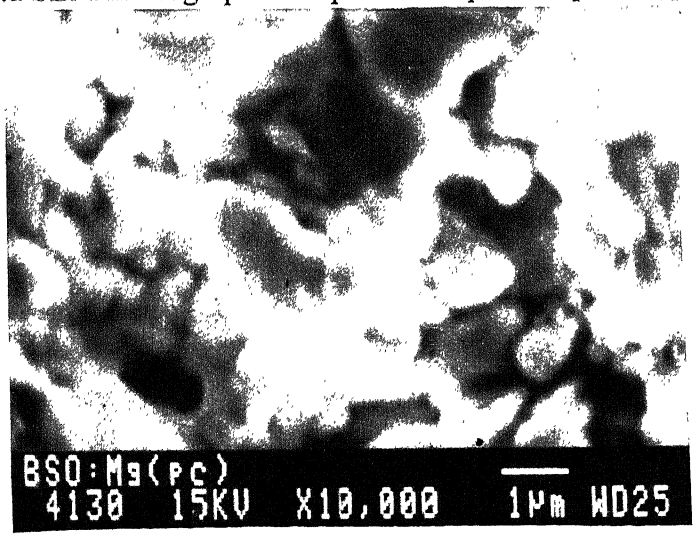

Fig 3.4.b SEM micrograph for BSO Mg pressed pellet (pc).

3.3 Density Measurements:

The density of the single crystals has been determined by the weight loss method (for experimental details see Section 2.5) and the value is found to be 9.21gm/cm^3, while the value reported in the literature [26] is 9.20gm/cm^3. By the same procedure the density of all the three types of pellets were determined The obtained result is given below.

(i) density of pure BSO pellet is found to be 92 % of the theoretical density BSO.

(ii) density of BSO:Mg pellet is found to be 93 % of the theoretical density of BSO.

(iii) density of BSO:Pr pellet is found to be 93 % of the theoretical density of BSO.

3.4 Complex Impedance Analysis:

The conventional method for electrical characterization of any material is to measure the ac conductivity at 1KHz frequency. While this method has been in use for a long time and continues to be used even today, it is now well recognized that this method is applicable only when the system under test is purely resistive. Strictly speaking, only metallic systems would fall in this category. For all other materials, the cell assembly, i.e the sample + electrode + leads, represents a complex impedance involving resistance and reactance / capacitance. The latter arises due to the capacitance between the electrodes and the sample , and the capacitance due to grain boundaries, etc. Thus the unknown sample is like a black-box consisting of resistance and capacitance in an unknown configuration. Hence to determine the resistivity / conductivity of the sample a complex impedance analysis has to be used.

Thus we have to study the impedance of the cell as a function of frequency with low amplitude ac but there still remains awkward problem of analyzing data involving several polarizations which may partially overlap in the frequency domain of interest or measurement. Thus the cell admittance is taken over a wide range of frequencies and then analyzed in the complex impedance / admittance plane. Complex impedance Z (ω) at an angular frequency ω can be expressed as:

$$Z(\omega) = Z' + jZ'' \qquad \text{.....(3.1)}$$

where Z' and Z'' are real and imaginary parts of the complex impedance. If the real part is plotted against the imaginary part, then the resulting locus shows distinctive features for certain combinations of circuit elements. In Section 1.10, it has already been described that for a standard combination of resistor R_p and a capacitor C_p in parallel, the equation of the curve is,

$$\left(Z' - \frac{R_p}{2}\right)^2 + (Z'')^2 = \left(\frac{R_p}{2}\right)^2 \qquad \text{.....(3.2)}$$

The above equation denotes the equation of a circle having radius $\frac{R_p}{2}$ and center at ($\frac{R_p}{2}$, 0). Thus the diameter of the circle gives directly the value of the dc resistance R_p. Thus we see how the complex impedance plot can help us to sort out the circuit configuration first and then determines the value of resistance / conductance. Generally speaking, the actual sample assemblies can often be modeled by a parallel combination of R_p and C_p. However, sometimes, more complicated configurations have to be employed to explain the observed complex impedance / admittance plots.

In fact the impedance analysis in our own BSO samples (both pc and sc) features two distinct sets of behaviour. At temperature of 400^0C and above, the impedance plots are semicircular, testifying that the sample is indeed equivalent to a parallel combination of R_p and C_p. However at lower temperatures, the impedance plots are more like straight lines with a constant phase angle very close to 90^0. More details of these results are presented below. A detailed analysis ultimately provides the following information; (i) dc conductivity, (ii) ac conductivity, (iii) dielectric constant ϵ' and loss ϵ'' and (iv) dielectric modulus M' and M''. In this section the results of impedance measurements on six different samples viz. BSO (pc), BSO:Mg (pc) and BSO:Pr (pc) and the corresponding single crystals, are presented and discussed.

3.4.1 High Temperature Behaviour:

It must be emphasized at the outset that the measurement of dc conductivity following complex impedance analysis demands much greater effort and patience. For instance, to obtain σ at just one particular temperature, magnitude of the complex impedance $|Z|$ and phase angle θ have to be measured atleast at 8 to 10 different frequencies in appropriate range, imaginary part $|Z| \sin\theta$, plotted as function of the real part $|Z| \cos\theta$, and appropriate curve fitted to the experimental data. As pointed out in Section 1.3.8, if the above plot turns out to be a semicircle signifying that sample - electrode assembly is equivalent to a parallel combination of an ideal resistor and capacitor, then the diameter of the semicircular plot yields the dc resistance (R_p) of the sample which then can be used to calculate the dc electrical conductivity (σ).

$$\sigma = \frac{1}{R_p}\left(\frac{l}{A}\right) \qquad \text{.....(3.3)}$$

where l is the thickness and A the area of cross section of the sample. Thus the conductivity is obtained at a particular temperature. The above procedure is to be repeated for each temperature at which σ is to be determined.

Typical complex impedance plots, $|Z|\cos\theta$ vs $|Z|\sin\theta$ are shown in Figs 3.5 and 3.6 for polycrystalline and single crystal samples respectively, at three different temperatures viz, 600^0C, 650^0C, 700^0C. Since six different samples have been examined at 10 different temperatures about 60 such plots were required to extract the dc conductivities. Of course all these results are not included in this Thesis.

It is observed in Figs 3.5 and 3.6 that the experimental data fits semicircular curve reasonably well and hence their diameter can be taken as dc resistance at that particular temperature. It is also noted that as the temperature of the sample increases, its resistance and hence the diameter of the semicircular plot decreases, as expected.

3.4.2 Low Temperature Behaviour:

It should however, be pointed out that at lower temperatures ($T < 400^0$C), the impedance plots ($|Z|\cos\theta$ vs $|Z|\sin\theta$) did not confirm to a semicircular one. Figs 3.7 and 3.8 show the results for ploycrystal and single crystal respectively, at two different temperatures 400^0C and 300^0C. The experimental data at 400^0C could still be fitted to a semicircle and hence dc resistance extracted, but the data at 300^0C for both polycrystal (Fig 3.7) and single crystal (Fig 3.8) fit nicely a straight line instead. This change over in

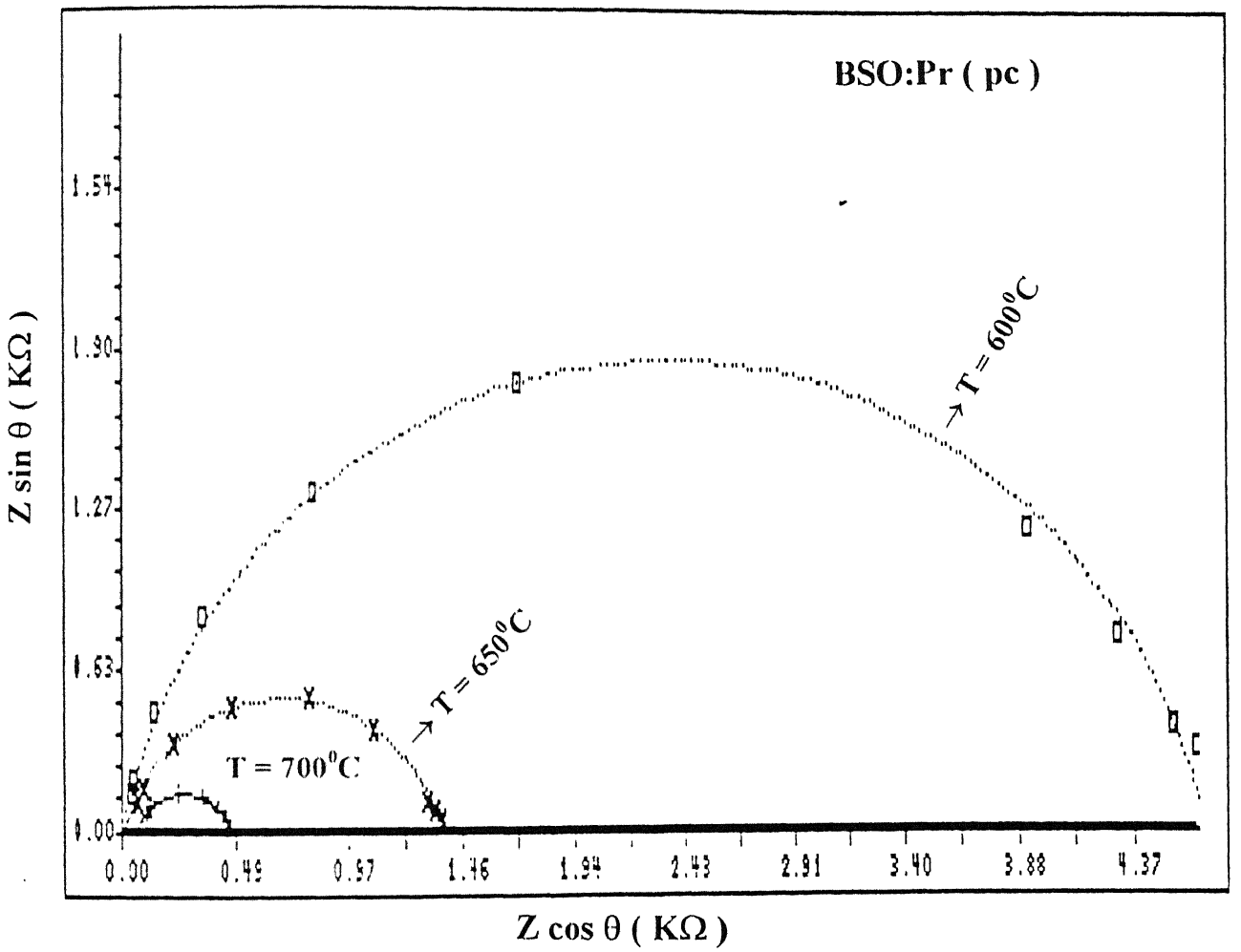

Fig 3.5 Complex Impedance plot for BSO:Pr polycrystal (pc) at three different temperatures 700^0C, 650^0C and 600^0C.

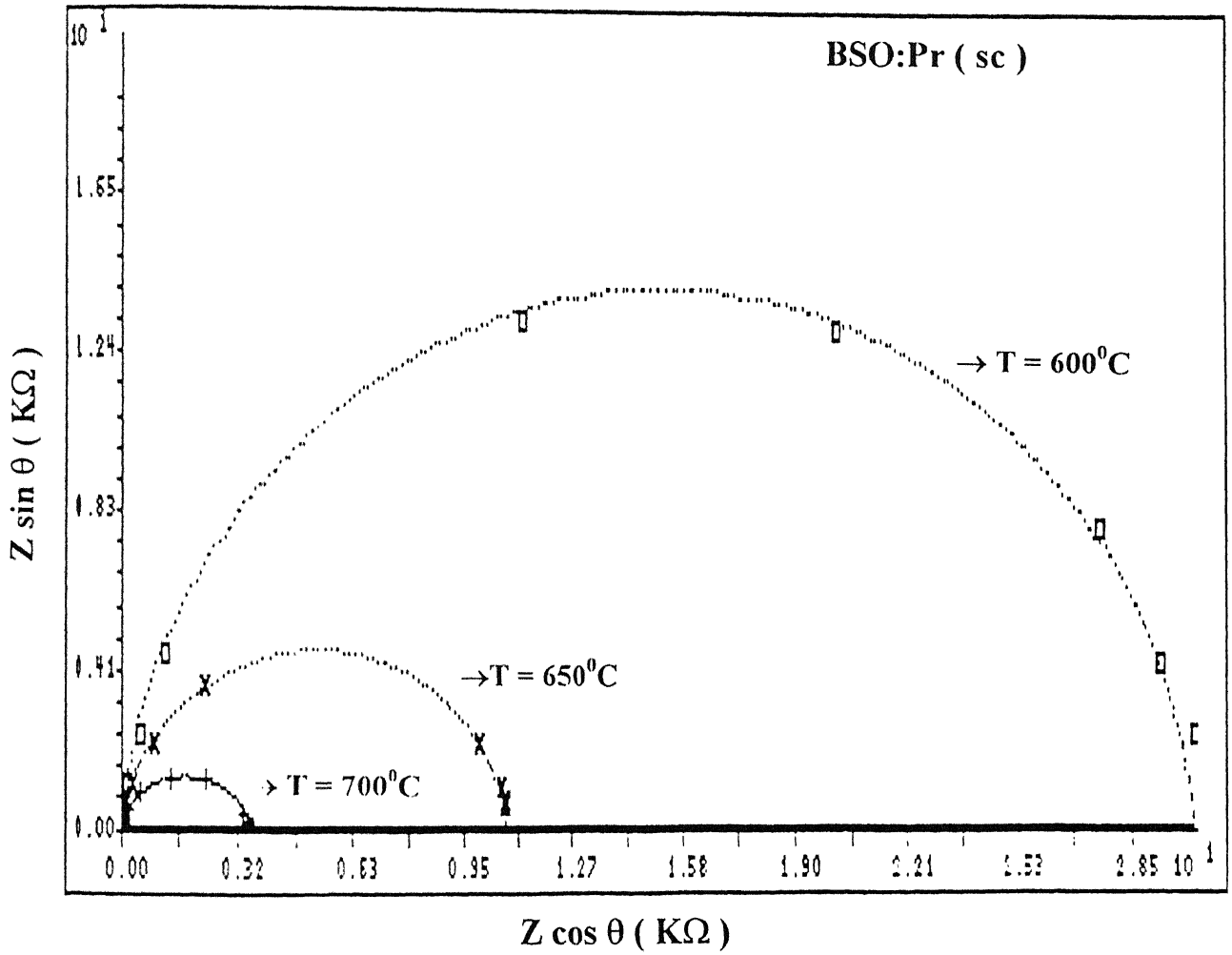

Fig 3.6 Complex Impedance plot for BSO:Pr single crystal (sc) at three different temperatures 700°C, 650°C and 600°C.

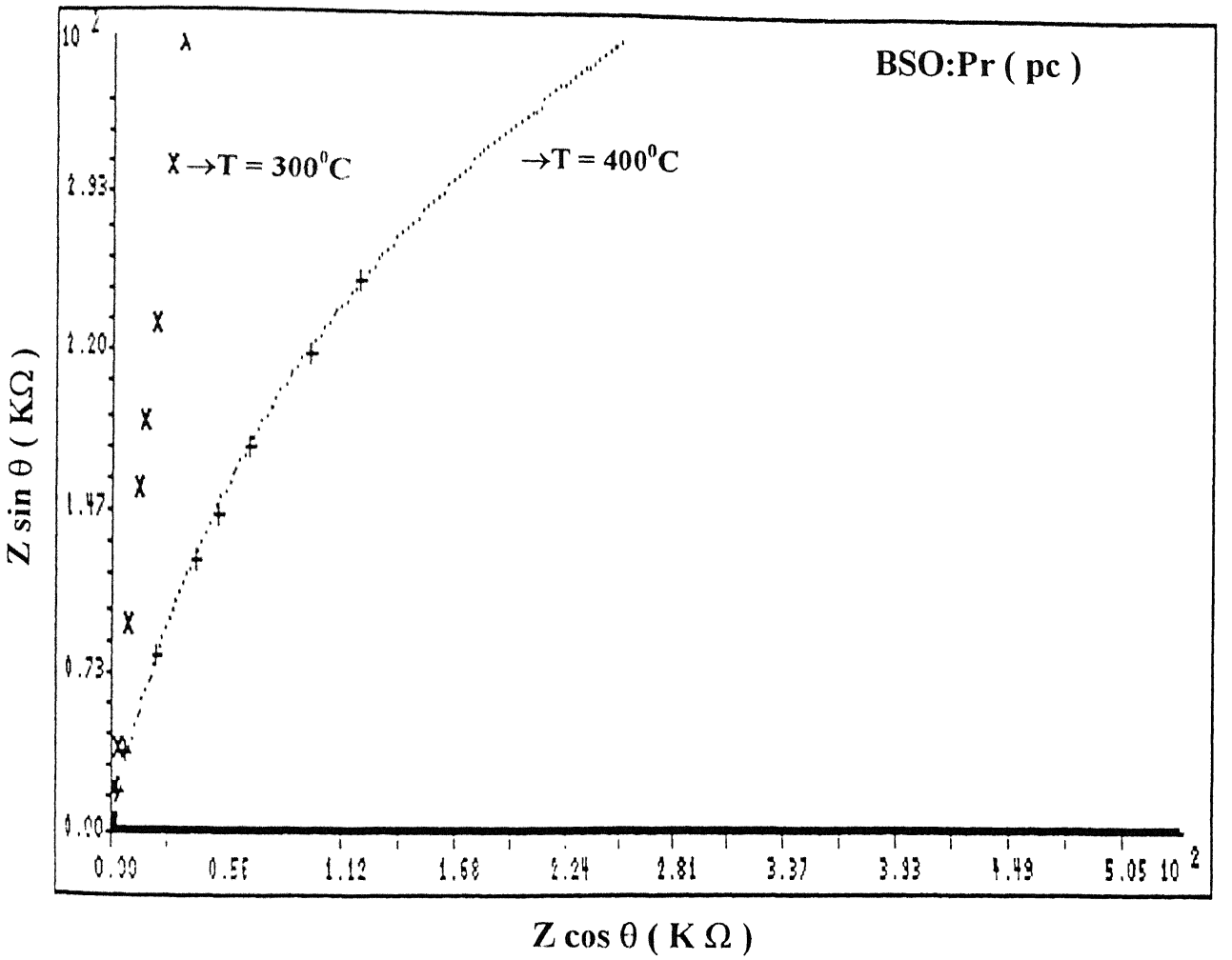

Fig 3.7 Complex Impedance plot for BSO:Pr polycrystal (pc) at two different temperatures 400^0C and 300^0C.

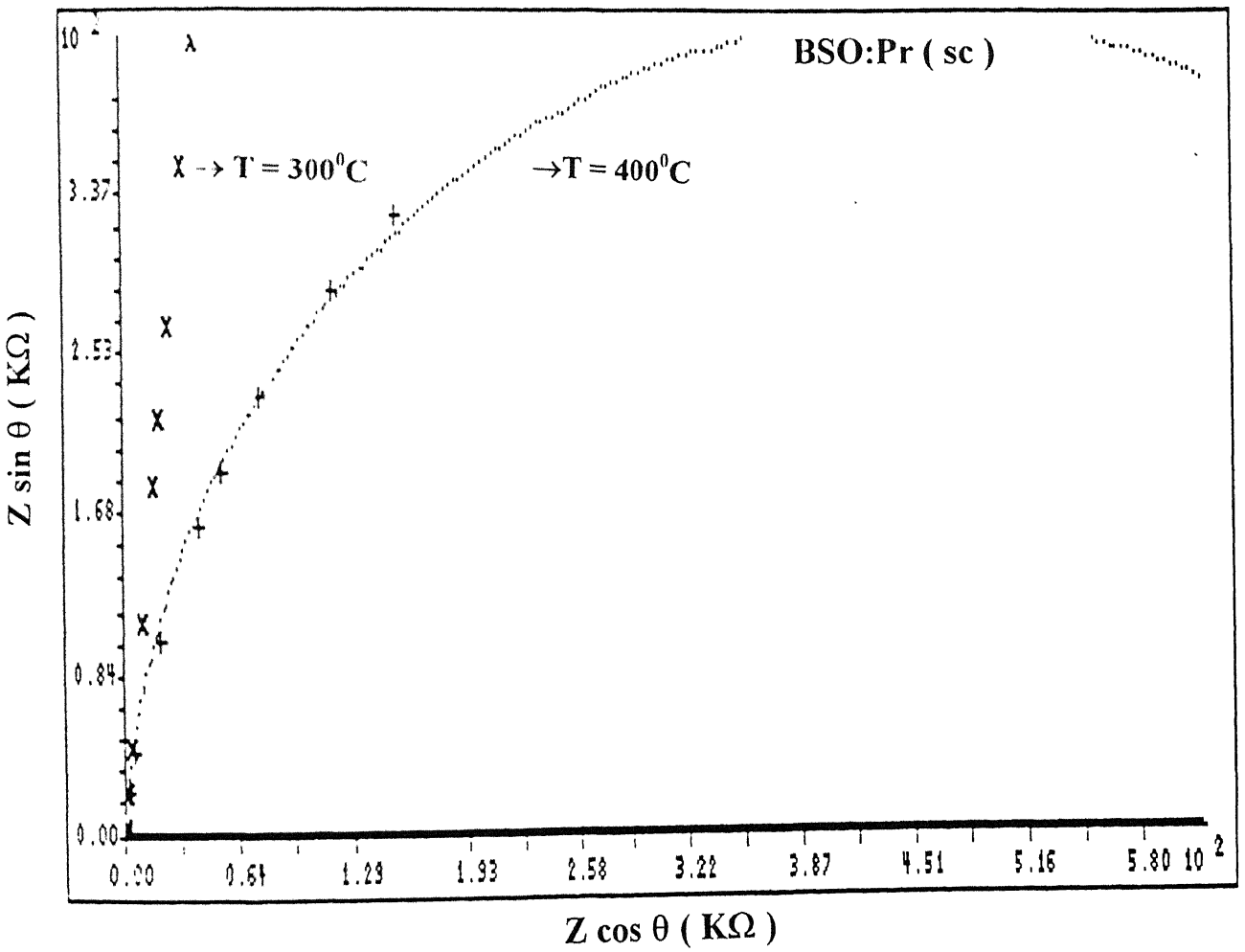

Fig 3.8 Complex Impedance plot for BSO:Pr single crystal (sc) at two different temperatures 400°C and 300°C.

impedance behaviour of the sample around 400^0C from semicircular to straight line is some what surprising.

One characteristic feature of the impedance plot at lower temperatures (below 400^0C) is that the phase angle 0 remains constant with frequency. Such a behaviour however is not uncommon in impedance spectroscopy, and is described by the so called "constant phase element" (CPE) whose complex admittance, in general, is given by [27];

$$Y = Y_0(j\omega)^n \qquad \text{.....(3.4)}$$

or $$Y = Y_0\omega^n e^{jn\frac{\pi}{2}} = Y_0\omega^n\left[\cos\left(\frac{n\pi}{2}\right) + j\sin\left(\frac{n\pi}{2}\right)\right] \qquad \text{.....(3.5)}$$

where n is a constant. If n = 0, the constant phase element (CPE) represents a pure resistor with $R = \frac{1}{Y_0}$. If n = 1, the CPE represents a pure capacitor, $C = Y_0$ and if n = -1, it is a pure inductor with $L = \frac{1}{Y_0}$.

The linear impedance behaviour observed at 300^0C (Figs 3.7 and 3.8) and indeed at any lower temperature, can be described as,

$$Z = |Z|\ e^{j\theta} = |Z|\ (\cos\theta + j\sin\theta) \qquad \text{.....(3.6)}$$

where $\theta \approx 84^0$ at 300^0C for both polycrystal and single crystal samples. A comparison of equation 3.6 with equation 3.5 yields the following value of n for our sample.

$$\theta = 84^0 = \frac{n\pi}{2} \qquad \text{.....(3.7)}$$

or $$n = \left(\frac{2}{\pi}\right)\left(\frac{84\times\pi}{180}\right) \approx 0.93 \qquad \text{.....(3.8)}$$

As discussed above a constant phase element (CPE) with n = 1 represents a pure capacitor. Thus the observed value of n = 0.93 at 300^0C suggests that the behaviour of our sample - electrode assembly at lower temperatures approaches to that of a pure capacitor.

This is not too surprising a result in view of the fact that as temperature decreases the resistance increases rapidly while the dielectric constant (see Section 3.4.2), and hence the capacitance remains practically constant, and thus the sample behaviour approaches that of an ideal (superinsulator) dielectric. Alternatively, examining the impedance (Z) of a parallel combination of R_p and C_p given by equation 1.14,

$$Z = \frac{R_p}{1+\omega^2 C_p^2 R_p^2} - j\frac{\omega C_p R_p^2}{1+\omega^2 C_p^2 R_p^2} \qquad \text{.....(3.9)}$$

in the limiting case $R_p >> \frac{1}{\omega C_p}$ or $R_p \to \infty$, we have

$$Z = \frac{1}{j\omega C_p} \qquad \text{.....(3.10)}$$

because the first term becomes vanishingly small. Thus to obtain the dc resistance of the samples at low temperatures (below 400^0C), a different procedure was adopted as outlined below. Essentially, in this temperature range, the real part of the admittance, Ycos0 , at an intermediate frequency 10KHz was taken as the conductance (reciprocal of resistance in parallel mode), i.e

$$\frac{1}{R_p} = Y\cos\theta \qquad \text{.....(3.11)}$$

or $$R_p = |Z|\sec\theta \qquad \text{.....(3.12)}$$

Hence $$\sigma = \frac{1}{R_p}\left(\frac{l}{A}\right) = Y\cos\theta\,\frac{l}{A} \qquad \text{.....(3.13)}$$

The electrical conductivity obtained as above may be termed average dc electrical conductivity.

3.4.3 DC Electrical Conductivity:

As pointed out earlier [28-32], the dc resistance (R_p) of each sample at various different temperatures extracted from the complex impedance analysis was used to calculate the dc conductivity (σ). Figs 3.9 to 3.11 show its variation as a function of inverse of absolute temperature ($^0K^{-1}$) for all the six samples investigated in this work, viz, BSO (pc), BSO:Mg (pc) and BSO:Pr (pc) and the three corresponding single crystals. Two distinct regions of electrical conduction are evident. We first discuss the high temperature (400^0C ~ 750^0C), so called intrinsic region of conduction which, for all the six samples, can be described by the well known Arrhenius equation of the form,

$$\sigma = \sigma_0 \exp\left(-\frac{E}{kT}\right) \qquad \text{.....(3.14)}$$

where σ_0 is the preexponential factor and E the activation energy for conduction. Assuming that BSO is essentially an electronic conductor, twice the activation energy (E) will give the band gap E_g i.e.,

$$E_g = 2E \qquad \text{.....(3.15)}$$

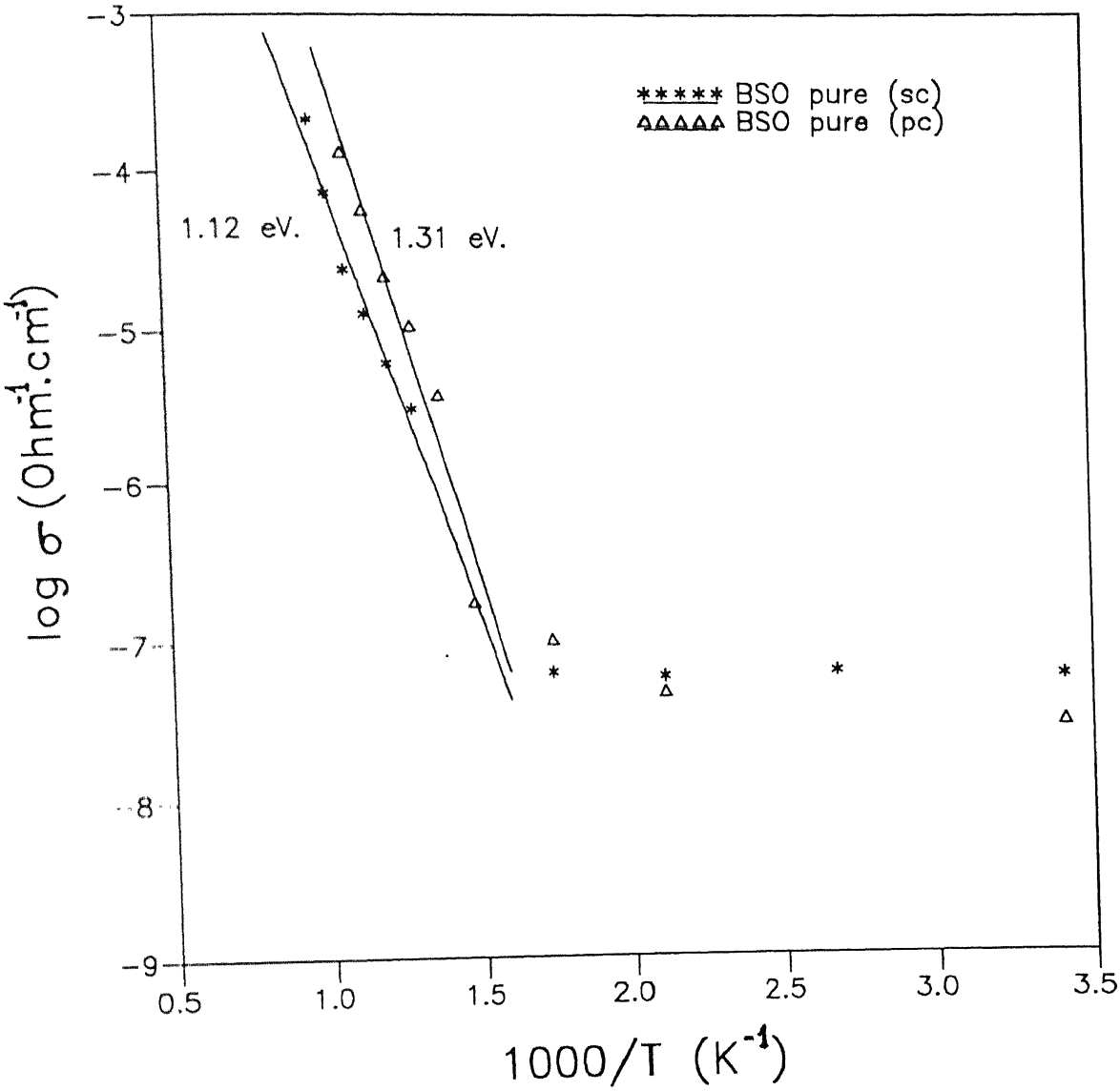

Fig 3.9 DC Electrical conductivity as function of inverse of temperature for pure polycrystalline (pc) and single crystal (sc) BSO samples.

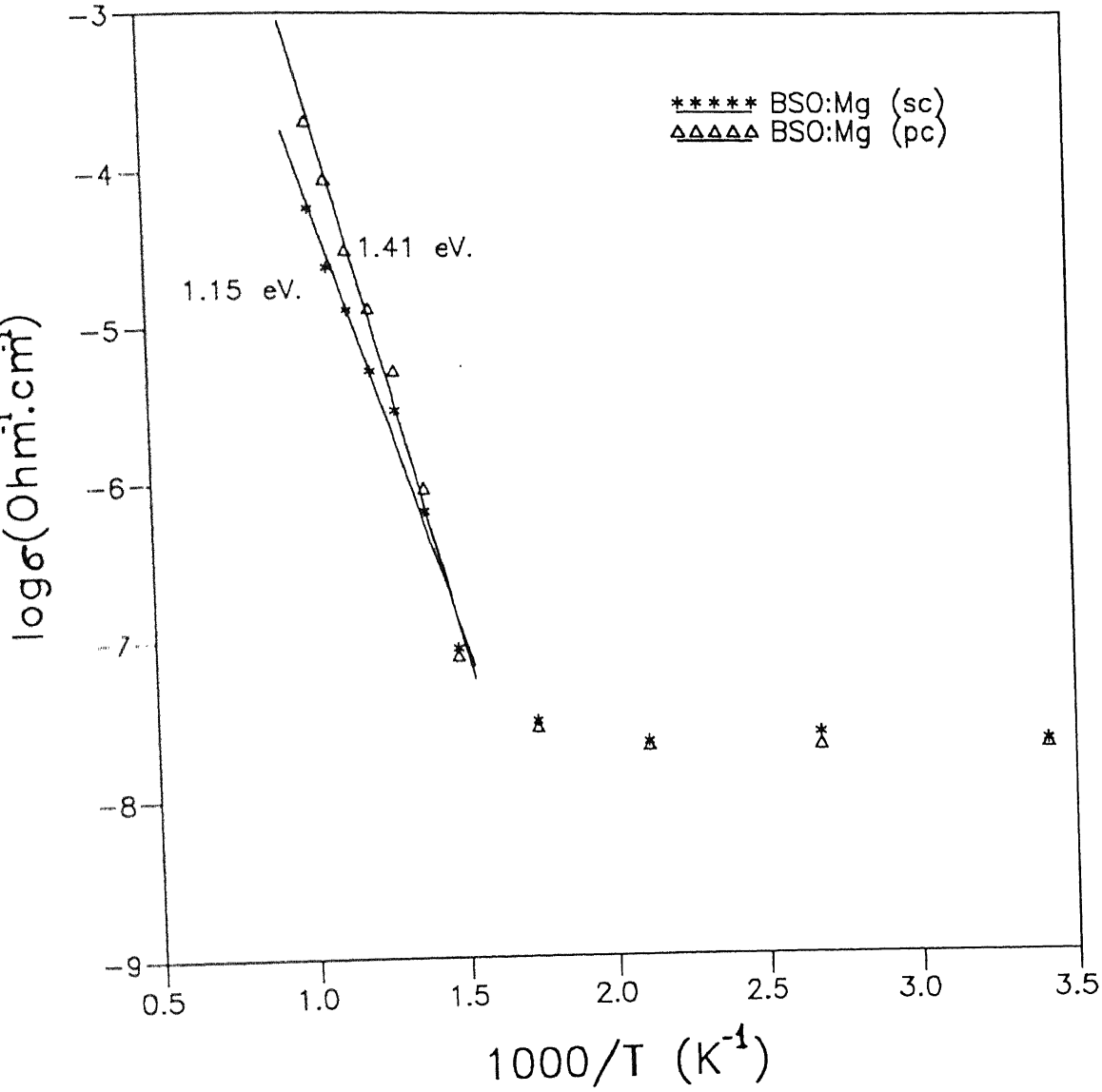

Fig 3.10 DC Electrical conductivity as function of inverse of temperature for polycrystalline (pc) and single crystal (sc) BSO:Mg samples.

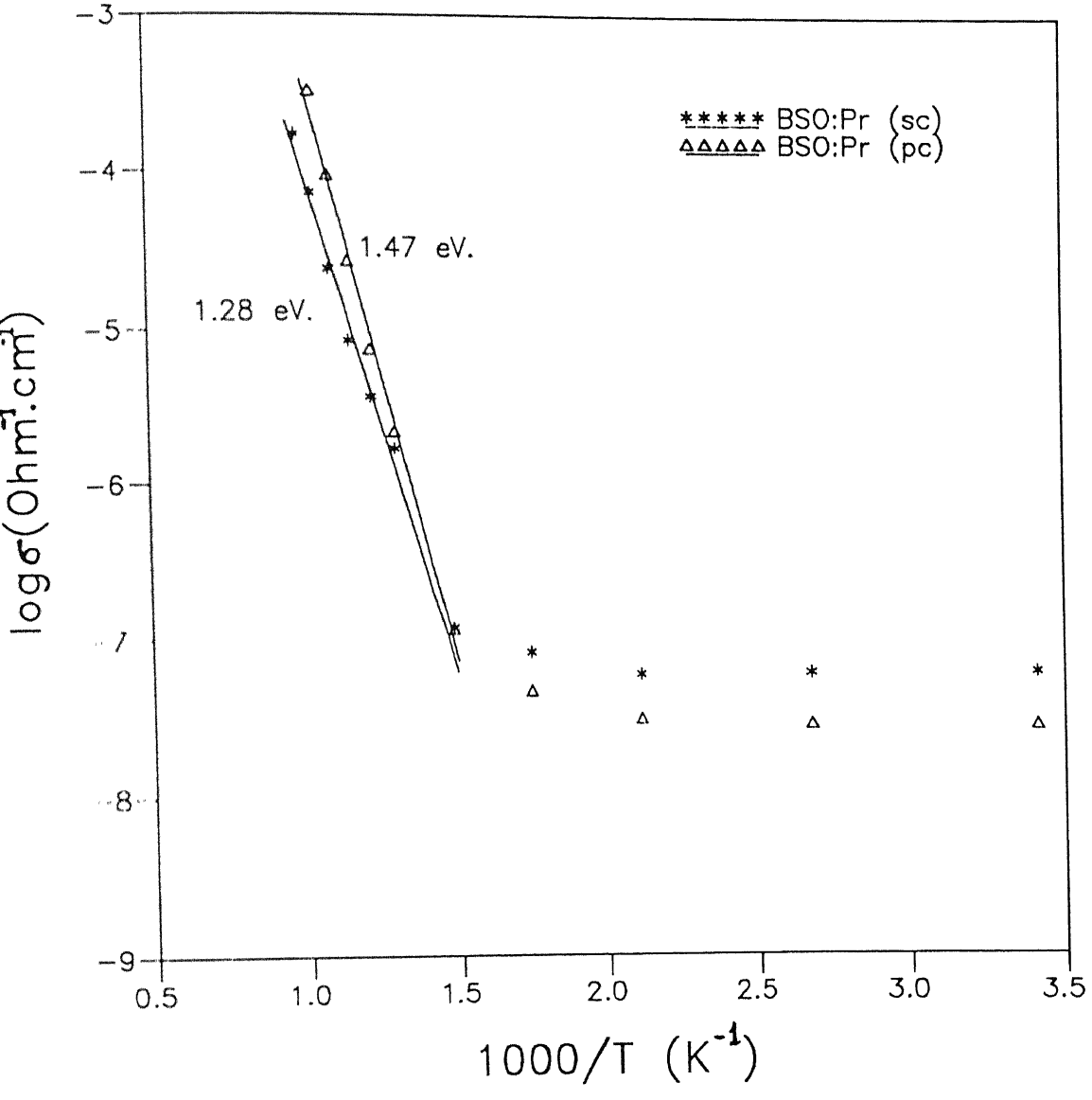

Fig 3.11 DC Electrical conductivity as function of inverse of temperature for polycrystalline (pc) and single crystal (sc.) BSO:Pr samples

The transport parameters σ_0 and E for all the six samples are summarized in Table 3.3. It is noted that the E values lie in the range 1.1 to 1.5 eV. It should be pointed out at this stage that BSO is essentially an insulator and hence samples' resistances were quite high, especially at lower temperatures, and thus the overall reproducibility was no better than ±10 %. Accordingly the calculated values of σ_0 and E are accurate only to within ±10 %.

Table 3.3

Transport Parameters of BSO

Sample	Temp. Range (^{0}C)	σ_0 ($Ohm^{-1} cm^{-1}$)	E (eV.)
BSO (pc)	400 ~ 750	3.4	1.3
BSO:Mg (pc)	400 ~ 750	3.7	1.4
BSO:Pr (pc)	400 ~ 750	4.0	1.5
BSO (sc)	400 ~ 750	1.7	1.1
BSO:Mg (sc)	400 ~ 750	1.8	1.2
BSO:Pr (sc)	400 ~ 750	2.4	1.3

A comparison of conduction behaviour between polycrystalline and single crystal samples reveals that the activation energy (and hence band gap, E_g) of the former is larger than that for the latter. Moreover, the samples containing impurities also exhibit higher activation energies than the undoped samples. While the pc sample shows a change of ~ 0.2 eV. from 1.3 eV for pure BSO to 1.5 eV. for BSO:Mg (2 mole %), the corresponding change for sc samples is also, perhaps coincidentally, by the same amount (see Table 3.3). In

view of the fact that the dopant concentration of ~ 2 mole% (Mg or Pr) is quite large, it is expected that the impurities modify the band structure and hence cause a change in the band gap / activation energy for conduction.

In view of the above discussion that impurities (MgO or Pr_2O_3) tend to increase the band gap, a somewhat higher value of E for pure BSO (pc) than that for pure single crystal is then to be expected because the nominally pure BSO powder sample may have a higher impurity content than the single crystal.

In the low temperature extrinsic region the electrical conductivity is practically independent of temperature for all the samples: pure as well as doped, polycrystalline or single crystalline samples. These results clearly suggest that the dopants or impurities do not affect the electrical properties in any significant manner (see Fig 3.12). However the effect of these impurities is clearly visible in terms of changes in the colour and optical activity of the crystals [33]. Moreover, literature report also show that the impurities do affect the colour and optical properties of the crystals. Thus our conductivity results shown in Figs 3.9 to 3.12, would suggest that either the impurities / dopants (MgO and Pr_2O_3) are electrically ineffective (eg, Ge in Si) or the impurities already present in the pure materials (pc or sc) are of the same variety and in far excess of what (2 mole %) is being added. Probably the first proposition seems more likely because the starting powders used for the preparation of BSO were of 5N purity.

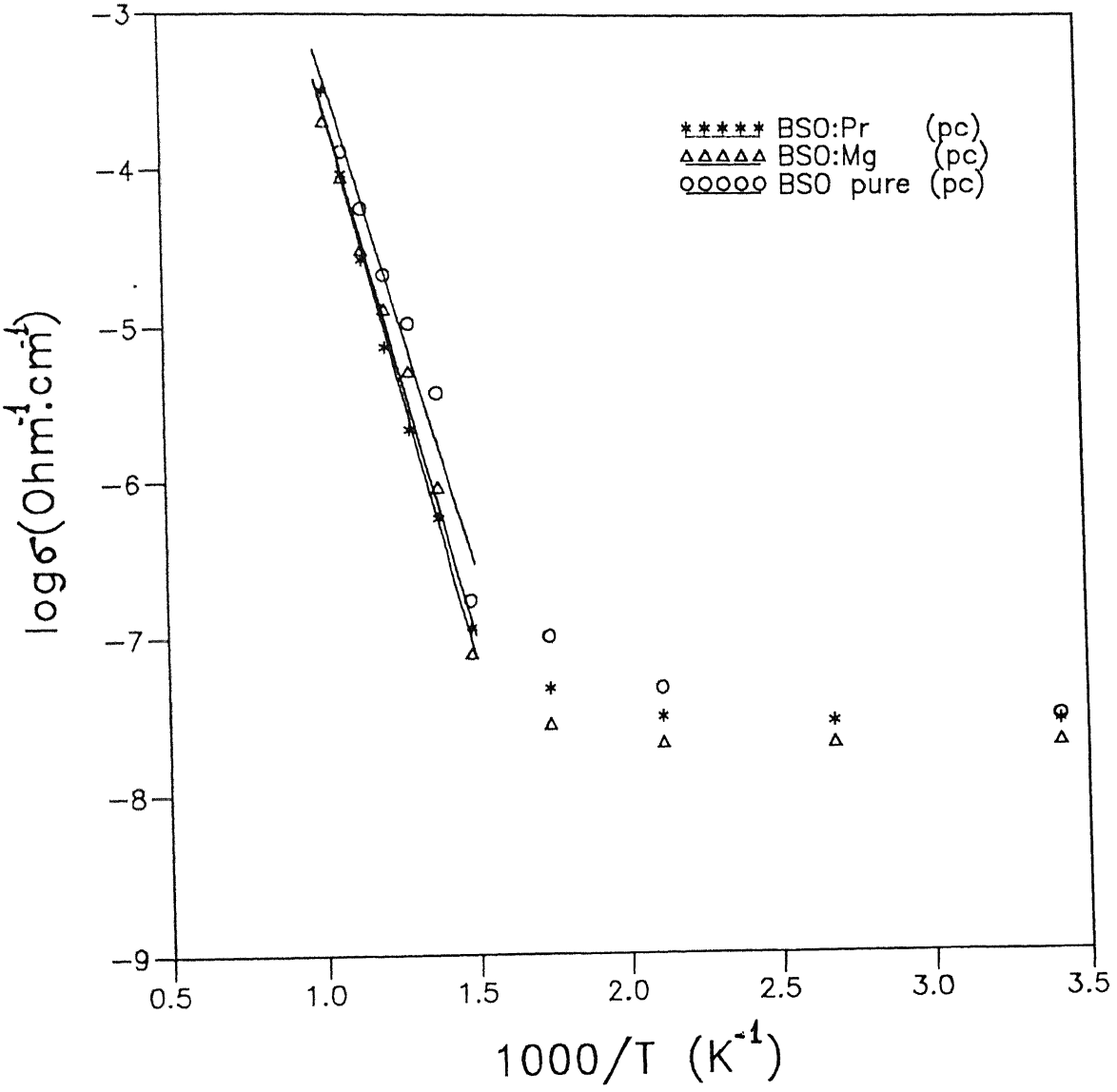

Fig 3.12 DC Electrical conductivity as function of inverse of temperature for BSO pure, BSO:Mg, and BSO:Pr polycrystalline samples.

3.4.4 AC Electrical Conductivity:

Fig 3.13 compares the variation of dc conductivity with that of the ac conductivity as a function of temperature. The procedure for obtaining dc conductivity has already been detailed in section 3.4.1. The ac conductivity (σ_{ac}), defined as the real part of the complex conductivity, is given by,

$$\sigma_{ac} = Y'\left(\frac{l}{A}\right) = Y\cos\theta\left(\frac{l}{A}\right) \qquad ..(3.16)$$

Y cos 0 is the real part the admittance, and is equal to $\frac{1}{R_p}$ if sample is equivalent to a parallel combination of R_p and C_p and hence its impedance plots are semicircular. It therefore follows that $\sigma = \sigma_{ac}$ under these conditions which are satisfied at $T \geq 400^0C$ for all the BSO samples (see Section 3.4.1). It is therefore not surprising at all that at high temperatures ($T \geq 400^0C$) the ac and dc conductivities have almost similar behaviour. At low temperatures, however, since n (= 0.94) very close to unity, σ could not be calculated and hence it cannot be compared with σ_{ac}.

3.5 Dielectric Properties:

The permittivity ϵ and the [34-35] relative permitivitty (or dielectric constant) ϵ_r are related to the permittivity of vacuum as given below,

$$\epsilon_r = \frac{\epsilon}{\epsilon_0} \qquad .. \qquad .....(3.17)$$

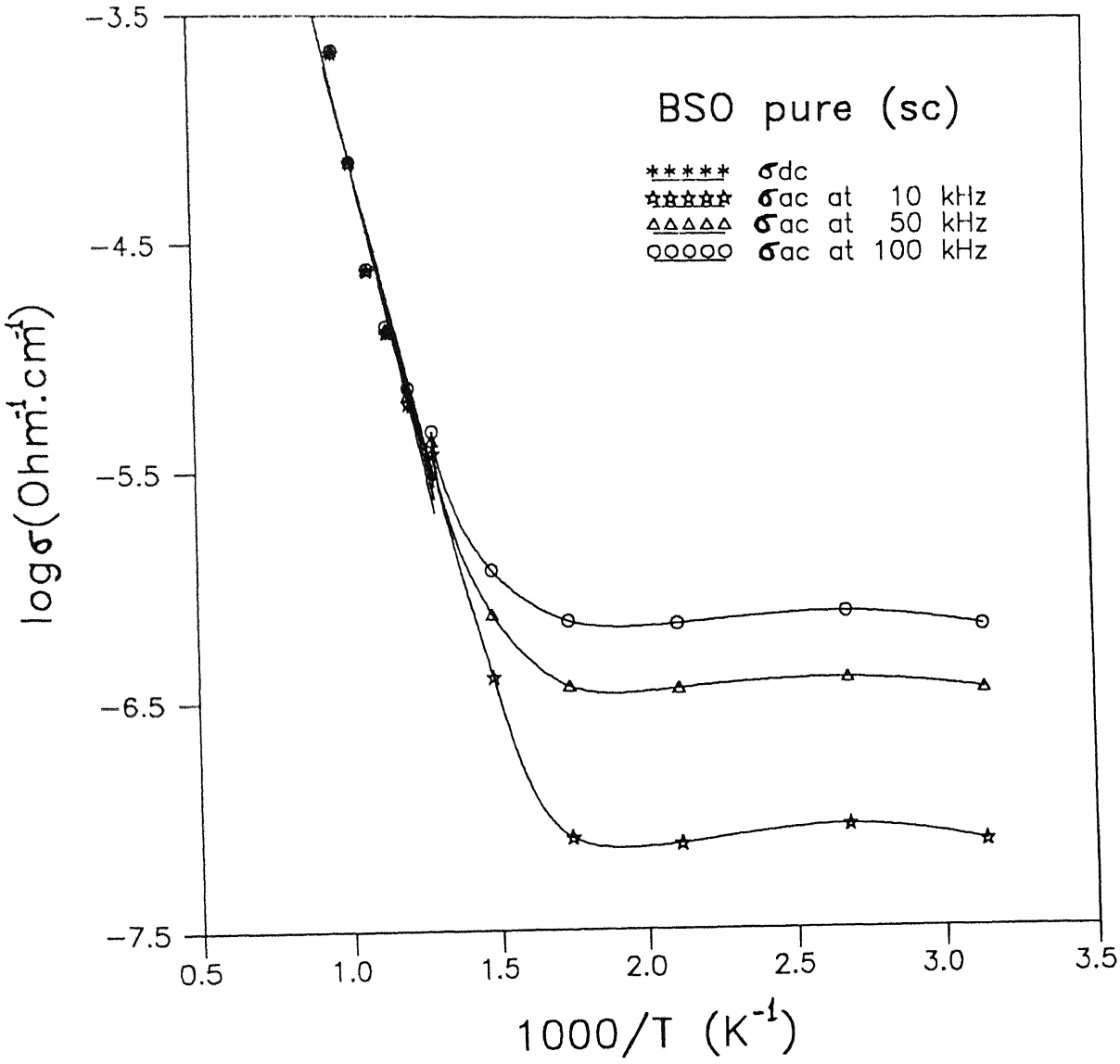

Fig 3.13 Variation of both ac and dc conductivity as function inverse of temperature for BSO pure single crystal (sc).

The complex dielectric constant (or relative permittivity) is defined as,

$$\epsilon_r^* = \epsilon' - j\,\epsilon'' = \frac{Y^*}{j\omega C_0} \qquad \text{.....(3.18)}$$

which yields

$$\epsilon' = \frac{Y''}{\omega C_0} = \frac{C_p}{C_0} \qquad \text{.....(3.19)}$$

and $$\epsilon'' = \frac{Y'}{\omega C_0} = \frac{1}{\omega C_0 R_p} \qquad \text{.....(3.20)}$$

The dielectric loss or dissipation factor (D) or loss tangent is defined as,

$$D = \tan\delta = \frac{\epsilon''}{\epsilon'} = \frac{1}{\omega C_p R_p} \qquad \text{.....(3.21)}$$

3.5.1 Dielectric Constant (ϵ'):

Typical variation of dielectric constant (ϵ') with the frequency of the applied field is shown in Fig 3.14. for BSO (sc), BSO:Mg (sc), and BSO:Pr (sc) at room temperature. The behaviour of the other three corresponding polycrystalline samples, viz, BSO (pc),BO:Mg (pc), and BSO:Pr (pc) was found to be similar. It is observed that the dielectric constant decreases uniformly as frequency increases, except at very high frequencies near 10 MHz which however is the extreme range of the HP - 4192 Impedance Analyzer and thus may not be highly reliable. It may be pointed out that the nature of the graph shown in Fig 3.14 is in fair agreement with the literature report [36]. However absolute values of ϵ' reported in literature are considerably lower than ours. It may be pointed out that their

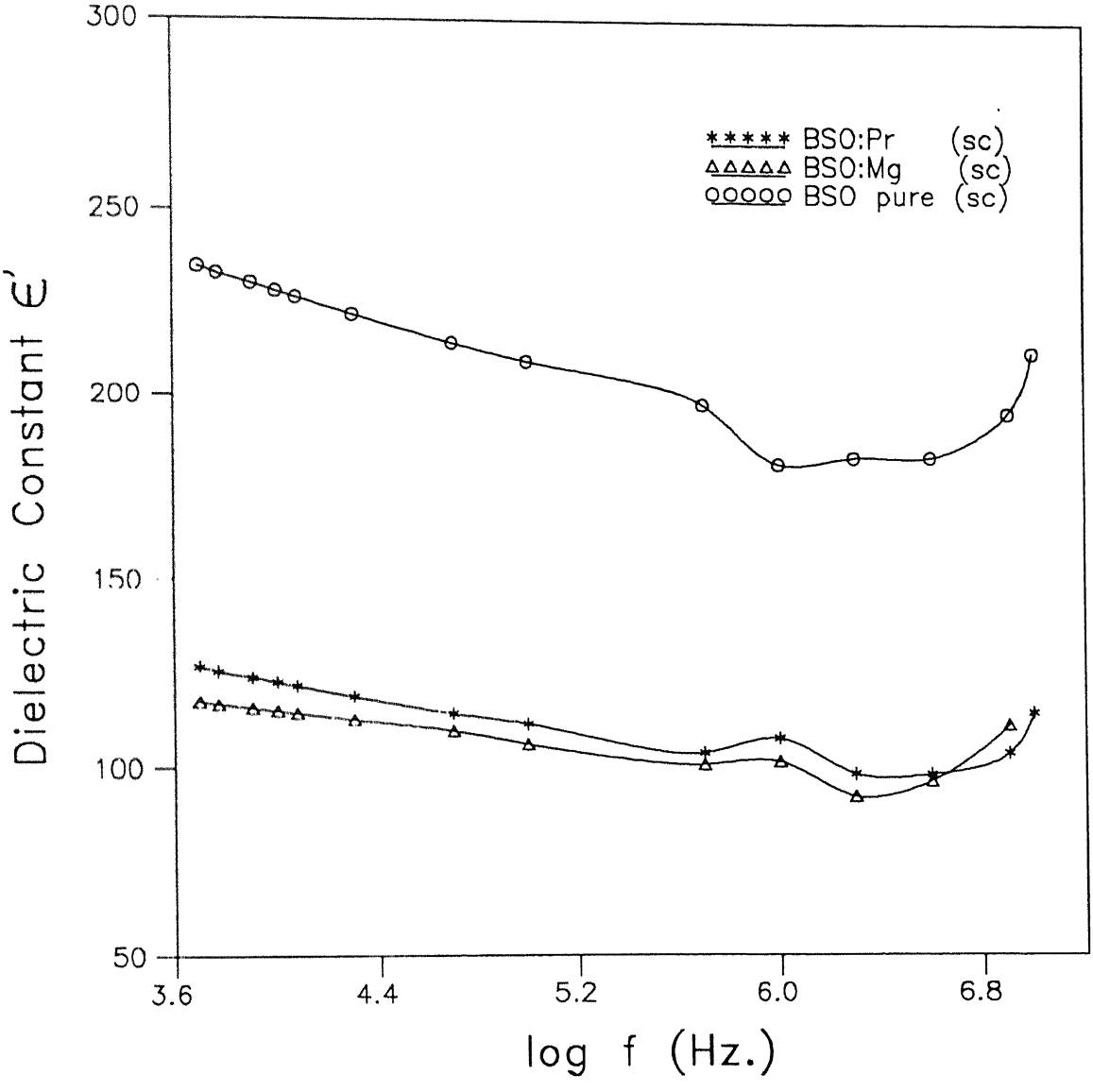

Fig 3.14 Variation of Dielectric Constant ϵ' as a function of frequency for pure BSO, BSO:Mg, and BSO:Pr single crystalline samples.

measurement was carried out on just one sample, BSO (sc), using an outdated instrument (GR 716 C).

The observed behaviour of ϵ' vs frequency (Fig 3.14) may be due to the involvement of different types dielectric polarizations like, (i) Space charge polarization, (ii) Dipolar / orientational polarization, and (iii) Ionic / atomic polarization.

If the permitivitty (ϵ') varies markedly with frequency the mechanism responsible for the variation can be characterized as a relaxation or as a resonance. A relaxation spectrum is generally characterized by a region of constant value, followed by a slow fall of ϵ' to a low value as frequency increases and a resonance spectrum shows a rapid fall from constant value. Since we do not observe a flat region because of measurements over a limited frequency range, the possible mechanism and corresponding relaxation frequency could not be obtained.

The variation of ϵ' as a function of $10^3/T$ is shown in Fig 3.15 for the sample BSO:Pr (sc) at four different frequencies: 5, 10, 50, and 100 KHz. It is noted immediately that the dielectric constant remains practically constant up to a temperature of 300^0C. As the temperature rises further, ϵ' starts increasing slowly upto 550^0C and beyond this temperature it increases rather rapidly. The behaviour below 550^0C, where ϵ' is either constant or changes slowly with temperature is a characteristic of ionic solids. The region where the dielectric constant increases rapidly as temperature increases is attributable to the space charge polarization of the thermally generated charge carriers due to the defects in the dielectric material.

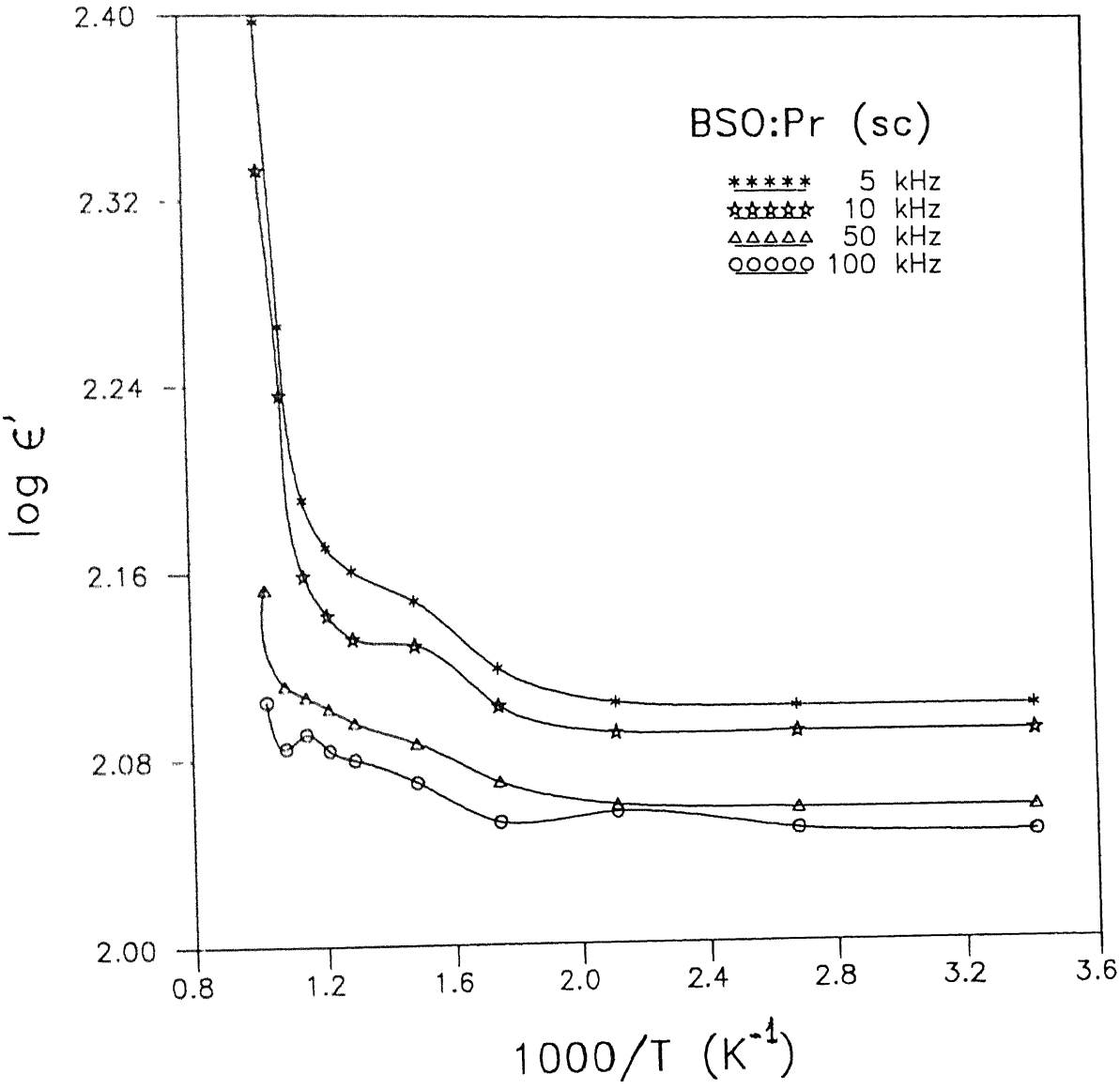

Fig 3.15 Variation of Dielectric Constant ϵ' as function of inverse of temperature for BSO:Pr single crystalline sample (sc) at four different frequencies.

As far as the effect impurities, Mg or Pr in BSO, is concerned, it is observed that the impurities tend to decrease the dielectric constant significantly (by about a factor 1.5 to 2). An explanation to this effect would demand a detailed knowledge of defect mechanism in BSO which is not available at present. However the behaviour of ϵ' with respect to frequency (Fig 3.14) remains unaltered, that is ϵ' decreases more or less uniformly as frequency increases. In order to compare the [37] dielectric constant (ϵ') of polycrystalline samples with that of a single crystal, the former may be thought of as a mixture of microcrystallites and air / vacuum filled voids. Thus total capacitance of the sample is the equivalent of two parallel capacitors, one air filled and the other filled by the material under examination, i.e,

$$\frac{\epsilon' \epsilon_0 A}{d} = \frac{\epsilon_s \epsilon_0 A_s}{d} + \frac{\epsilon_a \epsilon_0 (A - A_s)}{d} \qquad \text{.....(3.22)}$$

where ϵ_s and ϵ_a are dielectric constants of sample and air, and A_s and A are effective and actual areas of the sample respectively. Above equation can be written as

$$\epsilon' = (1 - \upsilon)\, \epsilon_s + \upsilon\, \epsilon_a \qquad \text{.....(3.23)}$$

where υ is the porosity fraction present in the sample. For single crystals, υ may be negligibly small. Since ϵ_s is generally larger than $\epsilon_a \approx 1$, as υ increases the observed value of ϵ' would decrease. That the dielectric constant for pellets is found to be smaller than that of single crystal is consistent with the above view.

3.5.2 Dielectric Loss:

The dielectric loss or loss tangent is defined as the ratio of ϵ'' to ϵ'. If ϵ' is practically constant, then ϵ'' itself is a measure of dielectric loss. Fig 3.16 shows the variation of ϵ'', the imaginary part of the dielectric constant, as a function of frequency at room temperature for BSO pure single crystal as well as doped with 2 mole% of Mg and Pr. It is observed that ϵ'' decreases rapidly as frequency increases. This is a general behaviour observed for several dielectric materials including the oxides.

The sharp fall in the value of ϵ'' as frequency increases might suggest the presence of Debye - type relaxation at a frequency lower than the lowest frequency employed in the measurement (5 KHz). If so, then ϵ'' vs logf curve at a higher temperature should exhibit a maximum so that the relaxation frequency corresponding to the peak frequency should be clearly identifiable.

However, these plots at higher temperatures (550, 600 and 650^{0}C) have the same shape and features as that at room temperature (Fig 3.16). This leads us to conclude that there is no orientational polarization present in BSO, and hence its dielectric properties may be attributed to space charge and atomic / ionic polarization. The electronic polarization which is always present in all materials and makes only a relatively small contribution to the dielectric constant, cannot by itself explain the large values of ϵ' observed for BSO.

The effect of impurities is to decrease the value of ϵ'' to some extent though the nature of ϵ'' vs logf curves remains almost the same. As pointed out earlier, ϵ'' is a measure of dielectric loss which in turn depends on the conductivity of the material; larger the conductivity larger is the loss. Since the conductivity of the doped material is somewhat

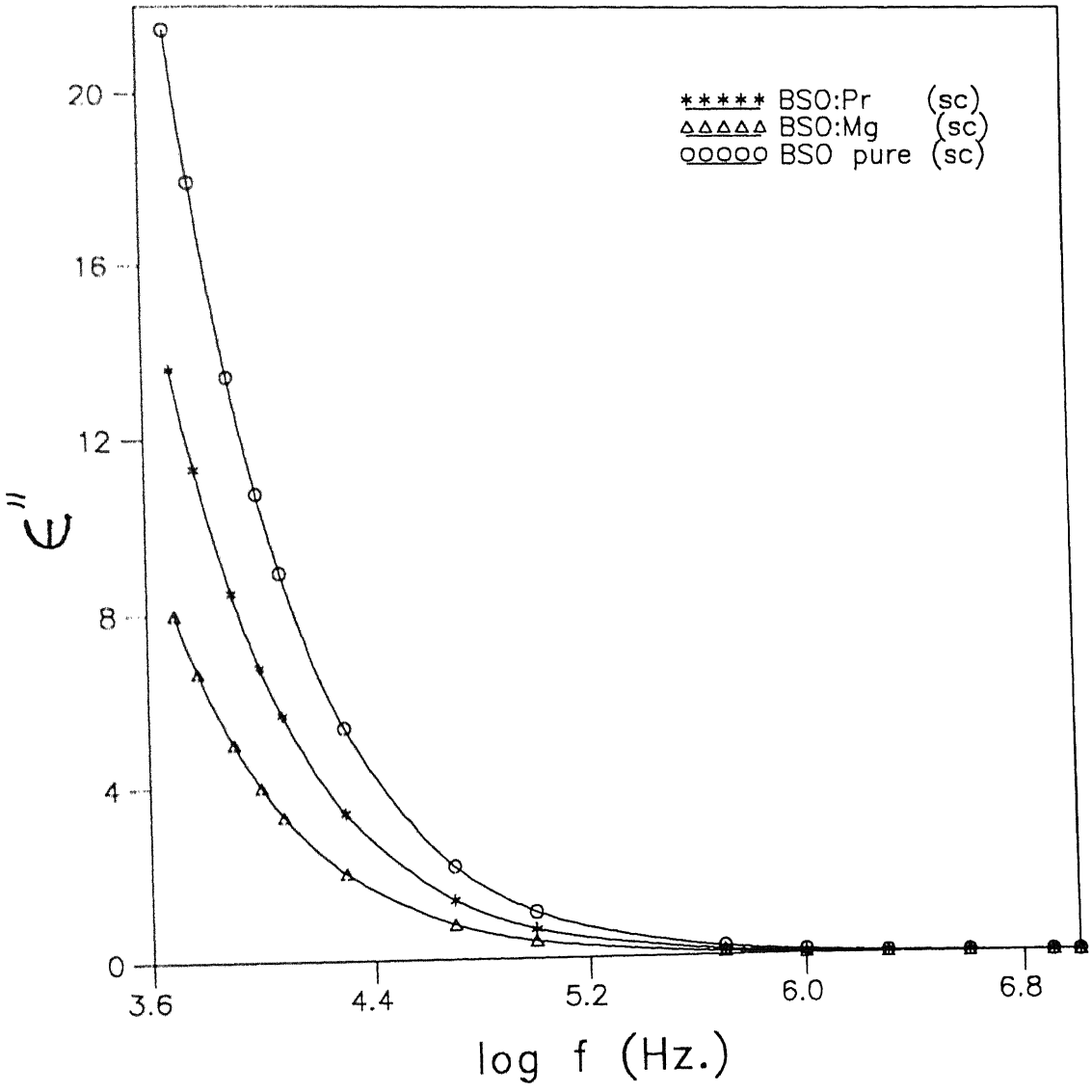

Fig 3.16 Variation of ϵ'' as function of frequency for both pure and doped BSO single crystalline samples.

lower than that for pure BSO (see Fig 3.12), lower values of ϵ'' for the doped material compared to that of pure BSO is therefore consistent.

Fig 3.17 shows the variation of log ϵ'' as a function of inverse of temperature at three different frequencies, viz 10, 50, and 100 KHz. It is noted that the observed log ϵ'' vs 10^3 / T behaviour comprises two distinct regions; A low temperature region (30^0C to 300^0C) wherein the ϵ'' is practically constant and a high temperature region (T > 300^0C) characterized by a relatively large slope. These results are consistent with the conduction characteristics (Figs 3.9 to 3.11), which is to be expected in view of the fact that the electrical conductivity is proportionally related to dielectric loss,

$$\sigma = Y' \frac{l}{A} = \omega \epsilon_0 \epsilon'' \qquad \text{.....(3.24)}$$

Fig 3.18 shows the variation of dissipation factor (D) which is same as loss tangent or dielectric loss, as a function of inverse of absolute temperature for BSO:Pr (sc) at three different frequencies, viz., 10, 50, and 100 KHz. The nature of these curves is basically similar to those of log ϵ'' vs 10^3 / T (Fig 3.17) and log σ vs 10^3 / T (Fig 3.11). Moreover this behavior is also to be expected in view of the fact that all these three parameters are closely related:

$$\sigma = Y \cos\theta \frac{l}{A} = \omega \epsilon_0 \epsilon'' = \omega \epsilon_0 \epsilon' D \qquad \text{.....(3.25)}$$

Thus for a fixed frequency, the electrical conductivity σ is proportional to ϵ'' which in turn is proportional to D especially at lower temperatures where ϵ' is practically constant.

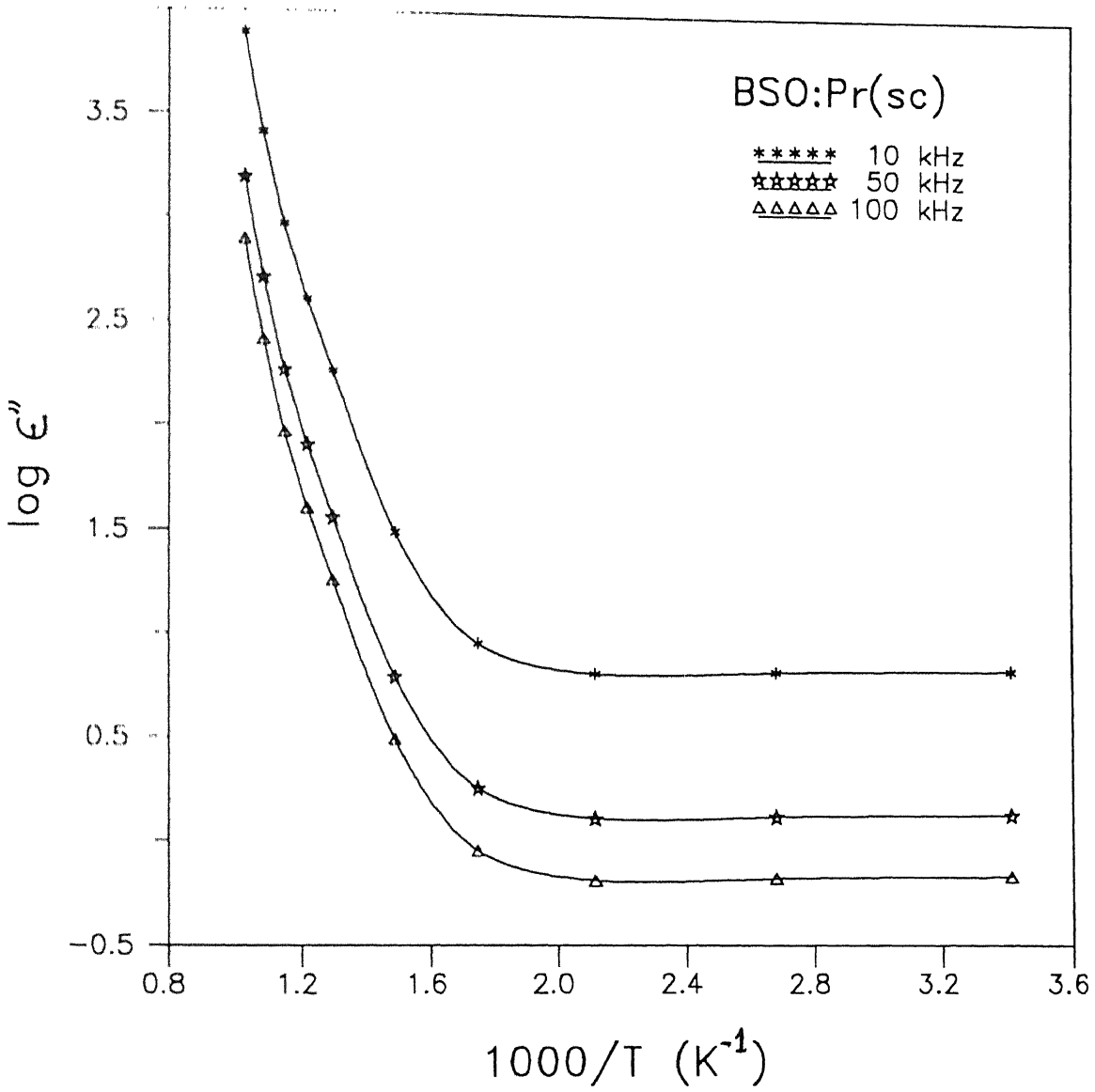

Fig 3.17 Variation of ϵ'' as function of inverse of temperature for BSO:Pr single crystal (sc) at three different frequencies.

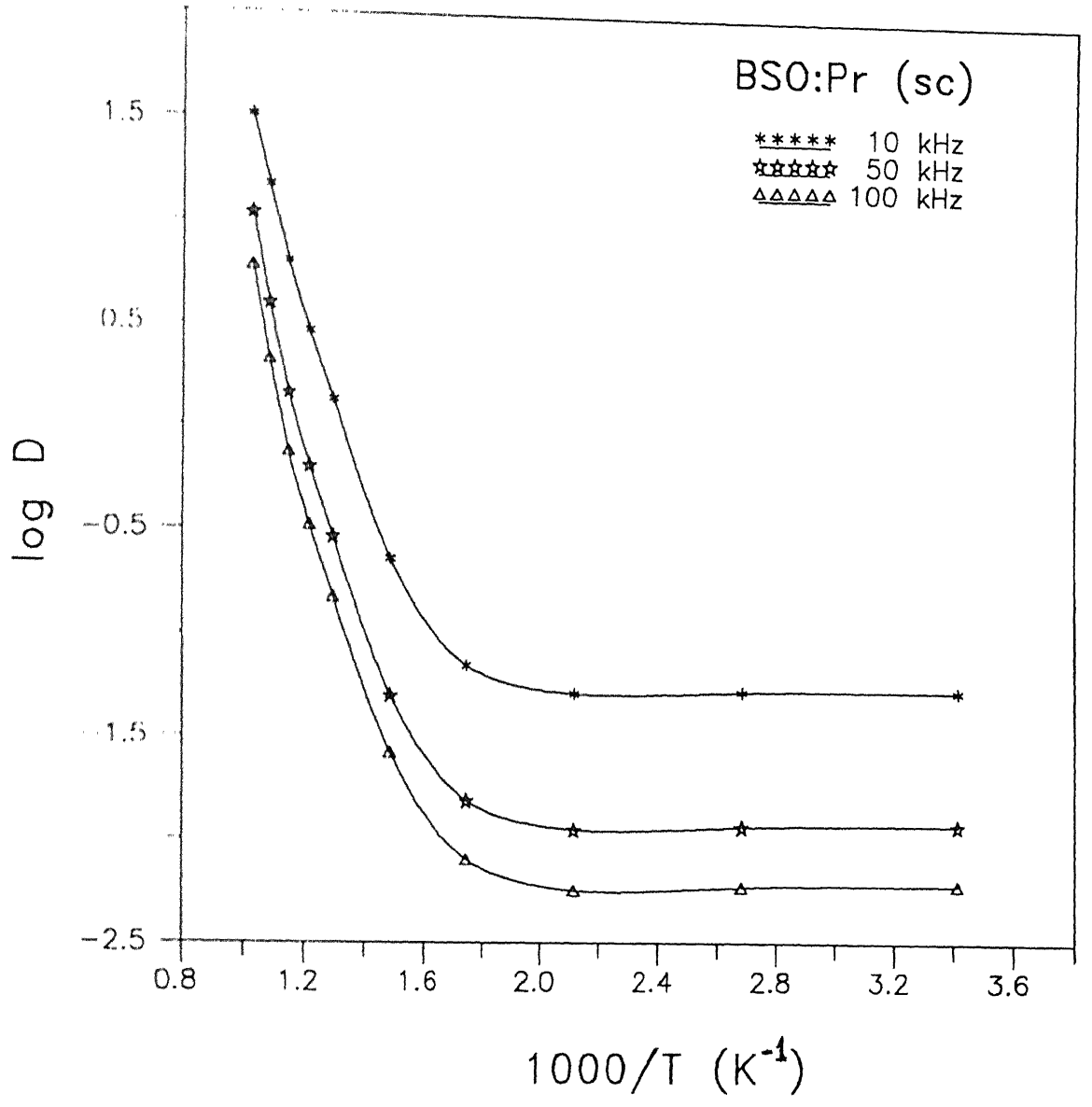

Fig 3.18 Variation of Dissipation factor (D) as function of inverse of temperature for BSO:Pr single crystal (sc) at three different frequencies.

3.6 Determination of Band gap:

Spectrophotometer experiment was performed in order to determine the band gap for all the three single crystals (see Section 2.6). It was found that for all the three single crystals the measured band gap was nearly 3eV. At the same time from the conductivity vs. temperature plot the calculated values of the band gap for all the three single crystals were found to be 2.2 – 2.6 eV., which was closely matched with the above result.

3.7 Summary and Conclusions:

(i) In all, six different samples have been prepared, viz. polycrystalline BSO (pc), BSO:Mg and BSO:Pr (pc), and BSO single crystal (sc), BSO:Mg (sc) and BSO:Pr (sc).

(ii) The samples have been examined by XRD to check the crystal structure, lattice constant etc. and also by SEM. The measured density is found to be close to the reported value.

(iii) All samples have been subjected to impedance measurement and analysis leading to dc electrical conductivity, dielectric constant and loss.

(iv) DC electrical conductivity has been reported over a wide temperature (30^0C to 750^0C) and frequency (5 KHz to 10 MHz) range. BSO is essentially an insulator at room temperature with a band gap of 2.97 eV. The dopants like Mg and Pr have little effect on the magnitude of conductivity, but they seem to change the band gap appreciably.

(v) BSO has reasonably high value of dielectric constant which decreases with increasing frequency as usual. The effect of impurities / dopants like Mg and Pr is only nominal as far as the dielectric properties are concerned. However literature reports indicate that these dopants change the optical properties, e.g., optical activity etc., considerably. In view of this discrepancy a re-examination of dielectric properties of BSO (pure and doped samples) may be worthwhile.

(vi) The dielectric loss measurements as function of frequency and temperature indicate the absence of Debye type relaxation process, and hence the dielectric behaviour of BSO is attributable to space charge and ionic polarization.

REFERENCES

1. Serey Thai, J. Malowiki, "Effective non-linearity of BSO crystal and its application to optical limiting", Mem. Neural. Netw., (USA), 3, 399, (1994).

2. P. Clemaire, "Local Measurement System for Optical and Electro optic Characterization and Homogeneity Analysis of Photorefractive Sillenite Crystals", Opt. mater., 4, 182, (1995).

3. J. Khoury, M.Cruinin, "Grating Competition for charge carriers in Photorefractive BSO", J. Appl. Phys. (USA), 77, 7, (1995).

4.K. Magade and G . Brost ,"Investigation of the internal field in Photorefractive Materials and measurement of the effective Electro optic coefficient", J. Opt. Society, 12, 921, (1995)

5. G. Roosen, "Photorefractive Effect in BSO or BGO single crystals", 22, 1253, (1987).

6. M.V Shilova, "Kinetics of Photoconductivity in single crystals of BSO", 22, 1535, (1986).

7. P.D Foote, "Photorefractive Materials and their applications in Optical Image Processing", IEEE proc., 1, 83, (1986).

8. Y.R Shen, "The Principles of Nonlinear Optics", Wiley Publication, p - 56, (1977).

9. David. D. Nolte, "Photorefractive Effects and Materials", Kulwar Academic Publishers, p - 2, (1995).

10. Mason, "Crystal Physics of Interaction Process", Academic press, p - 23, (1966).

11. Ian. D. Raistric, "Application of Impedance Spectroscopy to problems in Solid state Ionics", Solid State Ionics, 18/19, 40, (1986).

12. B V. R Chowdari and R Gopalkrishnan, "Impedance and modulus spectroscopy of vitreous AgI-Ag_2O-P_2O_5 system", Solid State Ionics, 18/19, 438, (1986).

13. A. R Kulkarni and H. S Maiti, "Electrode Effects in Lithium conducting Oxyfluorophosphate Glasses", Solid State Ionics, 14, 309, (1984).

14. Bernard A. Boukmap, "A Package for Impedance / Admittance Data Analysis", Solid State Ionics, 18/19, 136, (1986).

15. J. Ross Macdonald, "Impedance Spectroscopy", Wiley Interscience Publication, p - 2, (1987).

16. M. L. Soni and J. Gupta, "A Course in Electrical Circuit Analysis", Dhanpat Rai & Sons publication, p-77, (1976).

17. W. I Archer, "Application of ac Impedance methods to Solid Electrolytes", Chemical Society Specialist periodical Reports, 7, 157, (1980).

18. "Dielectrics make the difference in practical capacitor qualities", A guide to designers for RCL measurements, part - 3.

19. Shiuli Gupta, "Ph.D. Thesis on Ionic Transport in PEG - MX polymeric Electrolytes", 59, (1994).

20. Y. Suematsu, "Optical Devices and Fibers", Japan Annual Reviews in Electronics, Computers, and Telecommunications", 11, p - 154, (1984).

21. Senlin Fu and Hiroyuki Ozoe, "Growth Characteristics of single crystal rods and fibers of BSO by the floating zone method", J. Appl. Phys., 11, p - 5968, (1995).

22. "Powder Diffraction File", published by JCPDS, USA, p - 100, (1985).

23. "Powder Diffraction File", published by JCPDS, USA, p - 22, (1985).

24. B. D Cullity, "Elements of X-Ray Diffraction", Addison - Wesley publishing company, Inc., p - 28, (1978).

25. C. Kittel, "Introduction to Solid State Physics", Wiely Eastern Ltd., p - 41, (1976)

26. "Development of BSO crystals for Optical Modulators", A Completion Report sponsored by DRDO, New-Delhi., (1991)

27. Shiuli Gupta, "Ph.D. Thesis on Ionic Transport in PEG - MX polymeric Electrolytes", 61, (1994).

28. John. P. Mcklevey, "Solid State Semiconductor Physics", Harper and Row publishers, p - 277,(1964)

29. N. F Mott and E. A Davis, "Electronic Process in non-crystalline materials", Clarendon Press, Oxford, p - 456, (1973).

30. James D. Pattersion, "Introduction to the theory of Solid State Physics", Addison Wesley Publishing Company, p - 292, (1971).

31. Richard. H. Bube, "Electronics in Solids", Academic Press, Inc., Harcourt Brace Publishers, p - 164, (1988).

32. Sinnott and J. Murice "The Solid State for Engineers", John Wiley and Sons, Inc., p - 356, (1958).

33. Dr K. V Rao, "Study of BSO group for Optical information Processing", A Completion Report, Sponsored by DST., p - 5, (1995).

34. A. J Moulson and J. M Herbert, "Electroceramics", Champan and Hall Ltd., p - 52, (1975)

35. J. C Andersson, "Dielectrics", Champan and Hall Ltd., p - 10, (1964).

36. J. Kuwata, "Dielectric Losses in BGO single crystals", Jpn. J. Appl. Physics, 20, 1609, (1981).

37.J. B Briks and J Hart, "Progress in Dielectrics", p - 943, (1971).